

Review

Investigating Iron-Sulfur Proteins in Infectious Diseases: A Review of Characterization Techniques

Md Kausar Raza ^{1,*}, Vivian Robert Jeyachandran ² and Sania Bashir ³ ¹ Department of Chemistry, The Pennsylvania State University, University Park, PA 16802, USA² Department of Biochemistry and Molecular Biology, The Pennsylvania State University, University Park, PA 16802, USA³ Centre for Interdisciplinary Research in Basic Sciences, Jamia Millia Islamia, Jamia Nagar, New Delhi 110025, India

* Correspondence: mkr01@psu.edu

Abstract: Iron-sulfur [Fe-S] clusters, comprising coordinated iron and sulfur atoms arranged in diverse configurations, play a pivotal role in redox reactions and various biological processes. Diverse structural variants of [Fe-S] clusters exist, each possessing distinct attributes and functions. Recent discovery of [Fe-S] clusters in infectious pathogens, such as *Mycobacterium tuberculosis*, and in viruses, such as rotavirus, polyomavirus, hepatitis virus, mimivirus, and coronavirus, have sparked interest in them being a potential therapeutic target. Recent findings have associated these [Fe-S] cluster proteins playing a critical role in structural and host protein activity. However, for a very long time, metalloenzymes containing iron-sulfur clusters have been prone to destabilization in the presence of oxygen, which led to a delayed understanding of [Fe-S] proteins compared to other non-heme iron-containing proteins. Consequently, working with [Fe-S] proteins require specialized equipment, such as anaerobic chambers to maintain cofactor integrity, and tools like ultraviolet visible (UV-Vis) spectroscopy, mass spectrometry, X-ray crystallography, nuclear magnetic resonance (NMR), electron paramagnetic resonance (EPR), Mössbauer spectroscopy and electrochemical characterization. Many of these [Fe-S] cluster proteins have been misannotated as Zinc-binding proteins when purified aerobically. Moreover, the assembly of these iron-sulfur cluster cofactors have not been fully understood since it is a multi-step assembly process. Additionally, disruptions in this assembly process have been linked to human diseases. With rapid advancements in anaerobic gloveboxes and spectroscopic techniques, characterization of these [Fe-S] cluster-containing proteins that are essential for the pathogens can open up new avenues for diagnostics and therapeutics.

Keywords: bioinorganic chemistry; iron-sulfur clusters; biophysical characterizations; tuberculosis; viral diseases



Citation: Raza, M.K.; Jeyachandran, V.R.; Bashir, S. Investigating Iron-Sulfur Proteins in Infectious Diseases: A Review of Characterization Techniques. *Inorganics* **2024**, *12*, 25. <https://doi.org/10.3390/inorganics12010025>

Academic Editor: Nunziata Maio

Received: 17 November 2023

Revised: 3 January 2024

Accepted: 4 January 2024

Published: 7 January 2024



Copyright: © 2024 by the authors. Licensee MDPI, Basel, Switzerland. This article is an open access article distributed under the terms and conditions of the Creative Commons Attribution (CC BY) license (<https://creativecommons.org/licenses/by/4.0/>).

1. Introduction

Iron-sulfur [Fe-S] clusters represent the most ancient bioinorganic cofactors, universally present across the spectrum of life, spanning bacteria, archaea, and eukaryotes [1]. Initially, their role was primarily of catalytic hubs within proteins, mainly participating in electron transfer functions integral to respiration and photosynthesis. Beyond their multifunctional roles in catalysis, sensing, and electron transport, the significance of [Fe-S] clusters have been increasingly recognized in diverse biological activities [2–4]. Nucleic acid metabolism plays a significant role in protein stability, conformation and catalysis, influencing DNA replication, repair, and RNA biosynthesis [5]. Several human diseases, including cancer, neurodegenerative diseases, tuberculosis, and viral diseases are linked to abnormalities in the iron-sulfur biogenesis machinery associated with these [Fe-S] clusters [6–9]. Redox-active [Fe-S] clusters, which play a crucial role in DNA processing enzymes, have been demonstrated to be present in repair and replicative RNA/DNA polymerases such as (MUTYH, XPD, NER) and primase, Pol α , Pol δ , and Pol ϵ), nuclease/helicase Dna2,

facilitating electron migration to support DNA-mediated charge transfer (DNA CT) [10–15]. Iron, copper, and zinc have different roles in biological systems due to their different chemical compositions and redox properties. Zinc has been utilized instead of iron in certain situations due to its similar size and coordination properties. For instance, iron-sulfur [Fe-S] clusters exhibit instability when exposed to small molecules, particularly molecular oxygen, unlike many other iron-containing metalloenzymes [16]. Meanwhile, redox-inactive zinc has been widely used as a cofactor in metalloproteins, as it has a tolerance towards oxygen and provides structural stability and functionality in various metalloproteins [17,18]. In fact, for a very long time, [Fe-S] clusters were misclassified as zinc finger proteins, later discovered to harbor [Fe-S] clusters through comprehensive laboratory analyses and advanced biochemical and biophysical, including spectroscopic, techniques [17–19]. This characteristic has contributed to a slower advancement in our understanding of [Fe-S] proteins. As we delve deeper into understanding these [Fe-S] clusters, a growing array of their structural variations and capabilities has emerged, offering insights into their relevance to human health [20]. They have recently been implicated in viral diseases like hepatitis b and coronavirus disease 2019 (COVID-19) [21–23]. These [Fe-S] clusters are pivotal for redox reactions and an array of vital biological mechanisms, such as iron homeostasis [24]. This review explores the biophysical characterization methods employed to elucidate the structural nuances of different [Fe-S] cluster types. Furthermore, it explores the potential applications of [Fe-S] clusters in developing therapeutic strategies for combating infectious diseases.

2. Types of [Fe-S] Clusters

Based on the particular protein or enzyme in which they are present, as well as the coordination environment given by nearby amino acid residues, [Fe-S] clusters can have a variety of configurations [1,10]. Due to their variable structural makeup, these clusters can play various roles in living organisms and are crucial for effectively operating several biochemical processes. We delve into a selection of these typical [Fe-S] cluster structures that have been primarily identified and studied in the context of infectious diseases:

1. [2Fe-2S] cluster: Two iron and two sulfur atoms combine to form one of the most basic [Fe-S] cluster formations. Usually, the sulfur atoms form a cluster with a diamond-like structure by tetrahedral coordinating with the iron atoms. Proteins involved in electron transport, such as ferredoxins, frequently have this cluster type (Figure 1) [25].
2. [3Fe-4S] cluster: Three iron atoms coordinate four sulfur atoms. The artificial models of [3Fe-4S] clusters have a linear structure of three iron atoms, whereas protein-imposed structural constraints promote the development of a cuboidal shape for the [3Fe-4S]¹⁺ cluster. They are vital enzymes required for metabolic processes, including nitrogen fixation and the citric acid cycle. (Figure 1) [26].
3. [4Fe-4S] cluster: Proteins involved in redox reactions and electron transport pathways frequently include it. This more significant cluster has four sulfur and iron atoms. Sulfur atoms act as the coordinators of the iron atoms in a mixture of cubane and tetrahedral geometries (Figure 1). Aconitase and succinate dehydrogenase are enzymes and proteins that frequently include [4Fe-4S] clusters in redox processes [27]. Apo-aconitase is essential for cellular iron sensing, especially when the cell has an iron shortage [28]. When there is a shortage of iron in the cells, apo-aconitase acts as an iron sensor without the iron-sulfur cluster. This protein changes structurally to sense when iron is becoming less available. Because of this alteration, the protein responds to the iron status of the cell by adjusting its activity. Apo-aconitase is critical in preserving iron homeostasis within the cellular environment by employing its [4Fe-4S] cluster to enhance the cell's sensitivity to changes in iron levels. In contrast, the radical S-adenosyl methionine (SAM) enzyme catalytic [4Fe-4S]¹⁺ cluster coordinated three cysteines with either a solvent ligand or an unidentified small molecule, forming a gated cluster [29].

The nomenclature of Fe and S clusters is often the stoichiometry arrangement stated in square brackets, e.g., [2Fe-2S]⁺ or [4Fe-4S]²⁺, with the formal charge as a superscript.

At cryogenic temperatures, the number of unpaired electrons in the electronic ground state is represented by the spin state (S). In these [Fe-S] clusters, electrons are typically delocalized across the iron (Fe) and sulfur (S) atoms of the cluster. The degree of the electrons' delocalization can be assessed using electron paramagnetic resonance (EPR) and Mössbauer spectroscopy [30,31]. Notably, the oxidation states in which Fe is available, such as Fe^{3+} , $\text{Fe}^{2.5+}$, or Fe^{2+} , have a significant impact on both its redox and electronic characteristics.

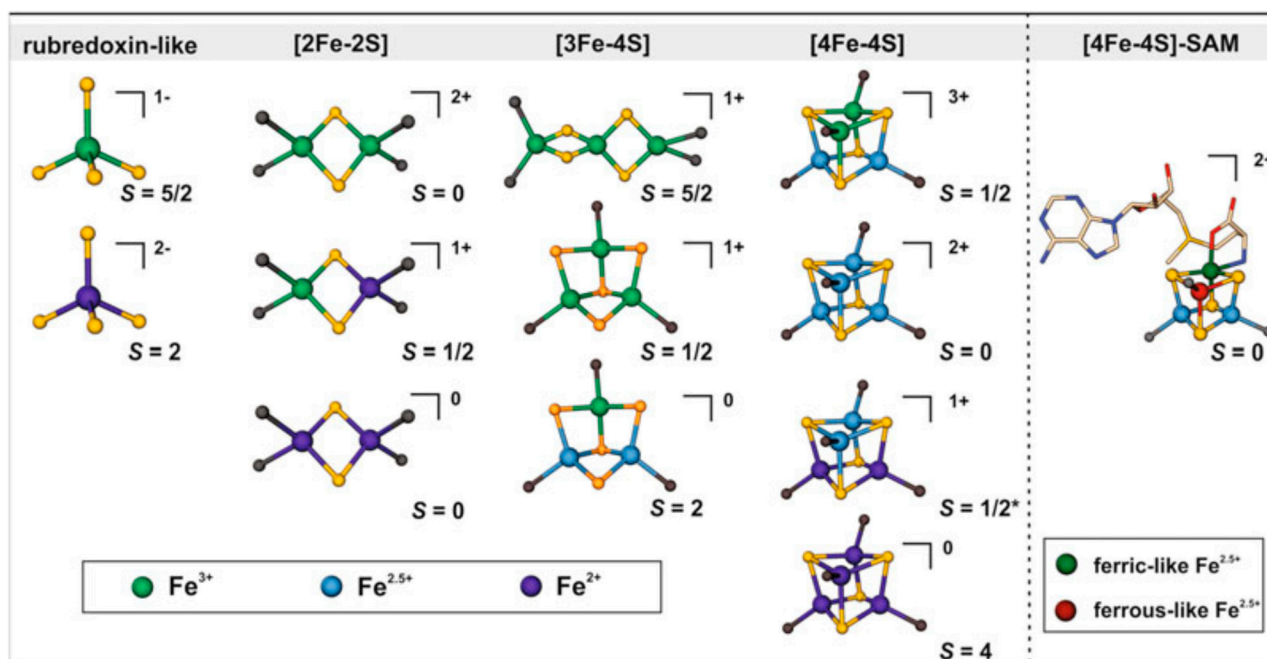


Figure 1. Typical [Fe-S] cluster types and their corresponding electronic properties, including SAM-bound [Fe-S] clusters, are shown with their oxidation states and spin, respectively. * represents additional higher spin of $[\text{4Fe-4S}]^{1+}$ clusters in ground states. Adopted from reference [31].

3. Different Characterization Techniques of [Fe-S] Clusters

3.1. Ultraviolet-Visible and Infrared Methods to Determine the [Fe-S] Cluster's Structure and Function

The ultraviolet-visible (UV-Vis) and infrared (IR) ranges can provide light on the electrical and vibrational characteristics of the [Fe-S] cluster. These methods identify the clusters' oxidation states, ligand interactions, and electronic transitions [32]. Different electronic transitions resulting from the unique arrangement of iron and sulfur atoms in each [Fe-S] cluster give rise to the absorption peaks and patterns in UV-Vis spectra. These optical properties are what make each [Fe-S] cluster unique. The structural differences and functions of various [Fe-S] clusters in biological systems and their identification and characterization are made more accessible by analyzing these spectrum patterns. For instance, the UV-Vis spectra of [2Fe-2S] cluster usually show characteristic peaks of 325–330 nm, 425 nm, 460 nm, and 550 nm in the oxidized form, depending on the coordination environment [33]. Spectrum features for a [3Fe-4S] cluster show broad absorption peaks between 380 and 400 nm [34]. Notable characteristics of a [4Fe-4S] cluster are unique, which are displayed at either 410 or 420 nm [32]. Mass spectrometry can determine the molecular masses and the composition of complete proteins and peptides that include [Fe-S] clusters [35]. Combining tandem methods with mass spectrometry may characterize the clusters' fragmentation patterns and ligand binding.

3.2. Structural Characterizations

Nuclear magnetic resonance (NMR) spectroscopy offers essential details about the immediate surroundings of [Fe-S] clusters in solution [36,37]. In NMR, chemical shift perturbation (CSP) is used to map protein–ligand and protein–protein interaction sites. A 2D-heteronuclear single quantum coherence (HSQC) spectrum of a ^{15}N or ^{13}C -labeled protein acquired in the presence and absence of [Fe-S] cluster can provide information on the coordination of the iron and sulfur atoms along with the neighboring amino acids they interact with. Clusters containing unpaired electrons can be studied using paramagnetic NMR methods. In paramagnetic NMR, the chemical shift is characteristically different and broader due to the hyperfine interactions between the electron and the nuclear spin. The hyperfine shift is the difference between a nucleus's chemical shift in a paramagnetic and a diamagnetic environment. Atoms closer to the paramagnetic source will have a more significant hyperfine shift.

X-ray crystallography is a potent method for figuring out the three-dimensional atomic structure of proteins and the amino acid residues that coordinate the [Fe-S] clusters [38]. Proteins that contain [Fe-S] clusters will have highly conserved cysteine-rich motifs. Radical SAM superfamily of enzymes, for example, have a highly conserved $\text{CX}_3\text{CX}_2\text{C}$ cysteine-rich motif that coordinates the three irons of a [4Fe-4S] cluster [29]. An amino acid residue does not coordinate with the fourth iron. S-adenosyl methionine (SAM) binds to the fourth iron and gets reductively cleaved to initiate a wide range of reactions [39]. Proteins that contain [Fe-S] clusters can also have a mix of cysteine and non-cysteine residues to coordinate the [Fe-S] clusters [40]. The non-cysteine ligands might be playing a crucial role in enzyme catalysis. The location of the iron and sulfur atoms, non-cysteine ligands, and essential amino acid residues required for catalysis can be precisely determined by crystallizing the protein and solving the structure using X-ray diffraction.

3.3. Biophysical Characterizations

Understanding the coordination environment, oxidation states, electronic characteristics, and functions in biological processes of [Fe-S] clusters requires various analytical approaches [41]. In this review, we have mainly discussed the characterization techniques on [2Fe-2S], [3Fe-4S], and [4Fe-4S] clusters, including electron paramagnetic resonance (EPR) and Mössbauer spectroscopy.

Studying [Fe-S] clusters containing paramagnetic species, such as clusters with unpaired electrons, require EPR spectroscopy [42]. It offers details on the clusters coordination geometry, oxidation states, and electronic structure. Systems like ferredoxins in oxidized states as $[\text{2Fe-2S}]^{2+}$ are EPR inactive; however, in the reduced state, they become EPR active ($S = 1/2$) with unique g -values 1.89, 1.94, 2.01 [43]. At the same time, [3Fe-4S] clusters have an EPR signal with average g -values of 2.0 for cubane type $[\text{3Fe-4S}]^{1+}$ ($S = 1/2$), whereas in the case of a linear $[\text{3Fe-4S}]^{1+}$ ($S = 5/2$), the g -values have been observed at 9.10, 4.30, and 4.15 [43,44]. In the case of a [4Fe-4S] cluster, the EPR features have been determined either for reduced $[\text{4Fe-4S}]^{1+}$ or oxidized $[\text{4Fe-4S}]^{3+}$ cluster ($S = 1/2$). The g -values for these types of clusters range from 2.04, 1.92, and 1.92 for reduced form and 2.12, 2.03, and 2.03 for oxidized states [45]. The g -values vary for these [Fe-S] clusters depending on the coordination environments and temperature conditions (Table 1).

Mössbauer spectroscopy primarily examines the electronic and magnetic characteristics of substances containing iron [24,25]. Isotopically labeled ^{57}Fe in [Fe-S] clusters unveils coordination surroundings and iron atoms' oxidation states. Two essential parameters, the isomer shift (δ) and the quadrupole splitting (ΔE_Q), reveal details on electron density at the nucleus, reflecting oxidation and spin states and ligand covalency. Isomeric shifts corresponding to oxidation state variations show a trend from Fe^{3+} to Fe^{2+} including $\text{Fe}^{2.5+}$. For example, the oxidized state of $[\text{2Fe-2S}]^{2+}$ clusters exhibit a single narrow quadrupole doublet ($\delta = 0.26$ mm/s) relative to iron and a 0.61 mm/s splitting (ΔE_Q) [43,46]. On the other hand, two quadrupole doublets ($\delta = 0.30$ mm/s and $\delta = 0.72$ mm/s) have been observed in the reduced state $[\text{2Fe-2S}]^{1+}$ [33,43]. The cubane type [3Fe-4S] cluster in ox-

oxidized form as $[3\text{Fe-4S}]^{1+}$ cluster displays a single quadrupole doublet ($\delta = 0.27$ mm/s) corresponding to equivalent three Fe^{3+} sites [33,47]. At 4K, zero-field Mössbauer studies of $[4\text{Fe-4S}]^{2+}$ show an isomeric shift ($\delta = 0.44$ mm/s) and broad quadruple splitting ($\Delta E_Q = 1.25$ mm/s) [22,30–32]. In the case of HiPIPs, the oxidized form of the $[4\text{Fe-4S}]^{3+}$ cluster has an isomeric shift $\delta = 0.28$ mm/s and $\delta = 0.40$ mm/s with quadruple splitting ($\Delta E_Q = 0.8$ mm/s and $\Delta E_Q = 1$ mm/s) based on the covalency. In contrast, the reduced form of the $[4\text{Fe-4S}]^{1+}$ has an isomer shift of $\delta = 0.60$ mm/s ($\Delta E_Q = 3$ mm/s) and $\delta = 0.48$ mm/s ($\Delta E_Q = 1$ mm/s). Moreover, the observed quadrupole splitting and isomeric shift values highly depend on temperatures, magnetic fields, and coordination environment settings inside the $[\text{Fe-S}]$ cluster (Table 1).

Table 1. Selected EPR g-values and Mössbauer parameters of different $[\text{Fe-S}]$ clusters.

Types of $[\text{Fe-S}]$ Cluster	S_{total}	EPRg (avg)	Mössbauer Parameters
^a $[2\text{Fe-2S}]$ -Oxidized	1/2	1.95	$\delta = 0.28$ and $\Delta E_Q = 0.61$
^b $[2\text{Fe-2S}]$ -Reduced	0	NA	$\delta = 0.30$, $\delta = 0.72$ and $\Delta E_Q = 1.06$, $\Delta E_Q = 3.15$
^c $[3\text{Fe-4S}]$ -Cuboidal	1/2	2.0	$\delta = 0.27$ and $\Delta E_Q = 0.62$
^d $[3\text{Fe-4S}]$ -Linear	5/2	5.85	$\delta = 0.28$ and $\Delta E_Q = \text{NA}$
^e $[4\text{Fe-4S}]$ -Native	NA	NA	$\delta = 0.44$, $\Delta E_Q = 1.25$
^f $[4\text{Fe-4S}]$ -Reduced	1/2	1.96	$\delta = 0.28$, $\delta = 0.40$ and $\Delta E_Q = 0.80$, $\Delta E_Q = 1$
^g $[4\text{Fe-4S}]$ -Oxidized	1/2	2.06	$\delta = 0.48$, $\delta = 0.60$ and $\Delta E_Q = 1$, $\Delta E_Q = 3$

^{a–g} Adopted from reference [24,25,43–47].

3.4. Electrochemical Techniques

The redox characteristics and electron transfer behavior of $[\text{Fe-S}]$ clusters in solution or on electrode surfaces were also investigated using electrochemical techniques such as cyclic voltammetry and potentiostatic/galvanostatic studies [11,48–51]. The intrinsic redox activity and charge transfer qualities of “redox protein” electrochemistry are mainly derived from the ligands, which include certain non-polypeptide groups and amino acid residues. Redox potentials of a wide range are induced around the metal center due to the ligand environment, the components of protein structures, the conditions of solvent exposure, including pH and hydrogen bond type, and electrostatic interactions obtained by many redox potentials. The primary functions of bacterial ferredoxins, which exist in the oxidation states (Fe^{3+} , 3Fe^{2+}) and (2Fe^{3+} , 2Fe^{2+}), are as electron relays in the forms $[4\text{Fe-4S}]^{1+}$ and $[4\text{Fe-4S}]^{2+}$. These two electrodes have potentials that are less than the typical hydrogen electrode (NHE), which ranges from -300 to -700 mV. An electron is transferred between $[4\text{Fe-4S}]^{2+}$ and $[4\text{Fe-4S}]^{3+}$ as a result of the oxidation of high potential iron-sulfur protein (HiPIP), (2Fe^{3+} , 2Fe^{2+}), and (3Fe^{3+} , Fe^{2+}) [6]. In contrast to NHE, the redox potential of the HiPIP $[4\text{Fe-4S}]^{3+/2+}$ cluster ranges between 65 and 400 mV (Figure 2).

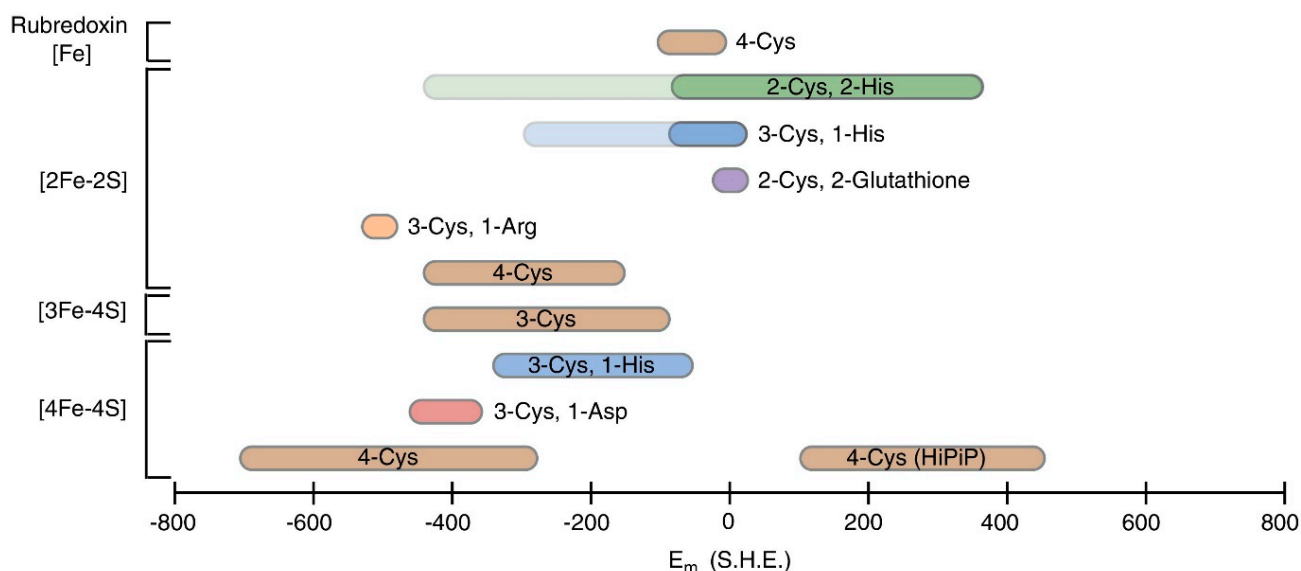


Figure 2. Illustrates the physiological potential window encompassing a wide range of [Fe-S] clusters with diverse redox potential values influenced by the ligand environment surrounding the metal center. [Fe-S] clusters sharing similar ligand environments are uniformly color-coded, with shaded regions denoting pH-dependent redox potentials. Adopted from reference [49].

4. [Fe-S] Cluster Functions in Viral Polymerases

The RNA- or DNA-based genetic material of viruses is replicated throughout their life cycle by viral polymerases [52]. These polymerases often rely on cofactors and metal ions, such as magnesium, to support their catalytic activity. As previously indicated, [Fe-S] clusters are more frequently found in proteins involved in electron transport, redox processes, and certain enzymatic activities [11]. Involvement of the [Fe-S] cluster in viral polymerases may occur in exceptional or unique circumstances. Still, it is not a well-known or common event in the context of viral replication. Metal ions including Zn^{2+} , Mg^{2+} , and Ni^{2+} operate as cofactors and support the structural stability, enzymatic activity, and function of numerous viral enzymes by enabling them to carry out their enzymatic activities [53,54].

4.1. Viperin—A [Fe-S] Cluster Containing Nucleotide Dehydratase

Viral infections in most cells activate an innate immune mechanism that results in the production of antiviral restriction factors [55,56]. Viperin, a virus-inhibitory protein linked to the endoplasmic reticulum and inducible by interferon, was one of the factors identified approximately two decades ago. Since then, viperin has been shown to act against various viruses via several hypothesized mechanisms. Although the enzyme was initially identified in 1997, and decade later, Shaveta et al. and Duschene et al. independently discovered that human viperin is a radical S-adenosylmethionine (SAM) enzyme is a viperin radical and contains the [4Fe-4S] cluster (Figure 3) [57,58]. The aerobic purification showed colorless protein, whereas anaerobically purified protein exhibited brown color that comes from presence of a [Fe-S] cluster (Figure 3E). The UV-visible spectrum of the reconstituted viperin showed characteristic bands at 325 nm and 415 nm, indicates the existence of the [4Fe-4S] cluster (Figure 3F). Moreover, CD and NMR spectroscopy corroborated the experimental data, demonstrating that viperin is a radical SAM enzyme with a [4Fe-4S] cluster [57]. EPR spectroscopy verified the catalytic reductive cleavage of SAM (Figure 3G) [58]. The native viperin sample that was reconstituted exhibited an isotropic EPR signal characterized by a $[3Fe-4S]^{1+}$ cluster. Spin quantification revealed that 0.09 spins/protein, approximately 10% of the iron present in the sample was detected by EPR, indicating that the rest is in an EPR silent state, most likely the $[4Fe-4S]^{2+}$ cluster (Figure 3G). Upon photo-reduction, the reconstituted native viperin exhibited axial EPR signal below 40 K with g-values

($g = 2.02, 1.92, 1.91; 0.28$ spins/protein) characteristic of $[4\text{Fe-4S}]^{1+}$ cluster (Figure 3G). Upon SAM addition to the reconstituted and photo-reduced samples, the EPR signal ($g = 2.03, 1.95,$ and $1.88; 0.28$ spins/protein) was consistent with SAM bound to the $[4\text{Fe-4S}]$ cluster (Figure 3G) [58]. Since viperin is implicated in nucleotide modifications, its characterizations with the help of biochemical/biophysical methods have opened up new avenues in antiviral therapeutics.

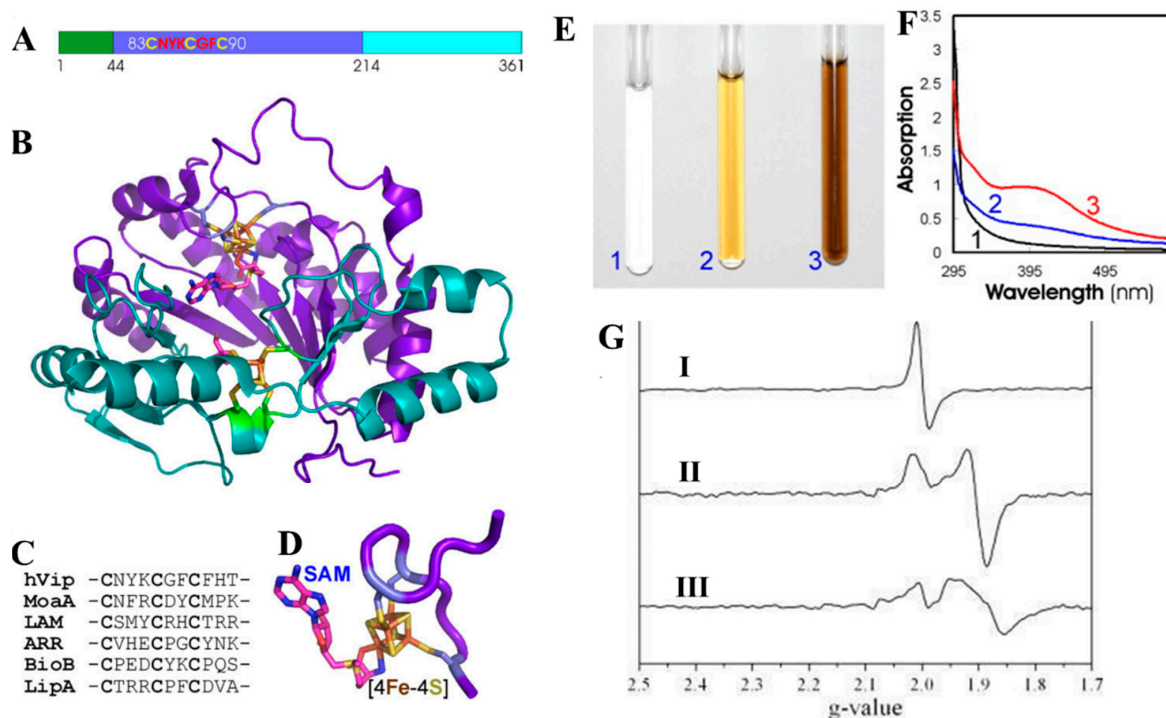


Figure 3. (A) Different domains of human viperin. (B) Crystal structure of MoaA in complex with SAM (PDB ID: 1TV8). (C) Conserved radical SAM cluster motif $\text{CX}_3\text{CX}_2\text{C}$. (D) SAM bound $[4\text{Fe-4S}]$ cluster from MoaA. (E) Purified viperin and its UV-Visible spectrum (F) under aerobic (1); anaerobic condition (2); and after reconstitution (3) [57]. (G) The X-band EPR spectrum of viperin after reconstituted (I), reconstitution and photo reduction (II), and photo reduction followed by the addition of SAM (III). Adopted from reference [58].

4.2. Nsp5—A $[\text{Fe-S}]$ Cluster Containing Protein That Modulates RNA Binding in Rotavirus

Rotavirus, a Reoviridae family member, causes gastroenteritis in animals [59]. Through viroplasm packing and viral genome replication, the infection spreads. The nonstructural proteins (nsp), nsp2, nsp5, and others, such as RNA-dependent RNA polymerase (RdRp) VP1 and core protein VP2, are present in viroplasms. NSP5 was recognized as the first viral metalloprotein required for the viral cycle and viroplasm development [60]. It is the first viral metalloprotein to bind to rotavirus groups A, C, and D. Poncet et al. purify the nsp5 protein in an aerobic environment [60]. It was observed that when the protein concentration increased, the pure nsp5 fragment transformed into a vibrant protein solution, with the color's intensity rising (Figure 4A). The samples were examined by various spectroscopy. The UV-Vis spectrum revealed 278 and 324 nm features and a wider absorption band at 422 nm, recognized as the signature bands for the $[2\text{Fe-2S}]$ cluster (Figure 4B). The susceptibility of the nsp5 $[\text{Fe-S}]$ cluster to oxygen was shown by the bands at 324 and 422 nm, whose peak intensities gradually decreased over time in an aerobic environment. The size exclusion column showed nsp5 eluting as a monomer (Figure 4C). Furthermore, the addition of dithionite in nsp5 showed an EPR signal ($g = 1.99, 1.96$ and 1.91), confirming the presence of a $[2\text{Fe-2S}]$ cluster (Figure 4D). They observed that the two conserved cysteines (C171 and C174) are essential for coordinating the iron-sulfur cluster units (Figure 4). Mutating these two cysteines to alanine (C171A and C174A) led to the loss of the UV-Vis

feature at 422 nm. Furthermore, upon double mutation, there was a total loss of UV-Vis bands at 322 nm and 422 nm, and the protein became colorless. Therefore, these two cysteines are the ligands for the [2Fe-2S] cluster. Since there are no other conserved residues, they propose that nsp5 exists as dimer with a [2Fe-2S] cluster coordinated by four cysteines at the dimeric interface. Single mutation of the [Fe-S] cluster facilitates the replication and packaging of the genome. They demonstrated how nsp5's [2Fe-2S] cluster influences the protein's propensity for binding single-stranded RNA, potentially indicating its role in viral replication.

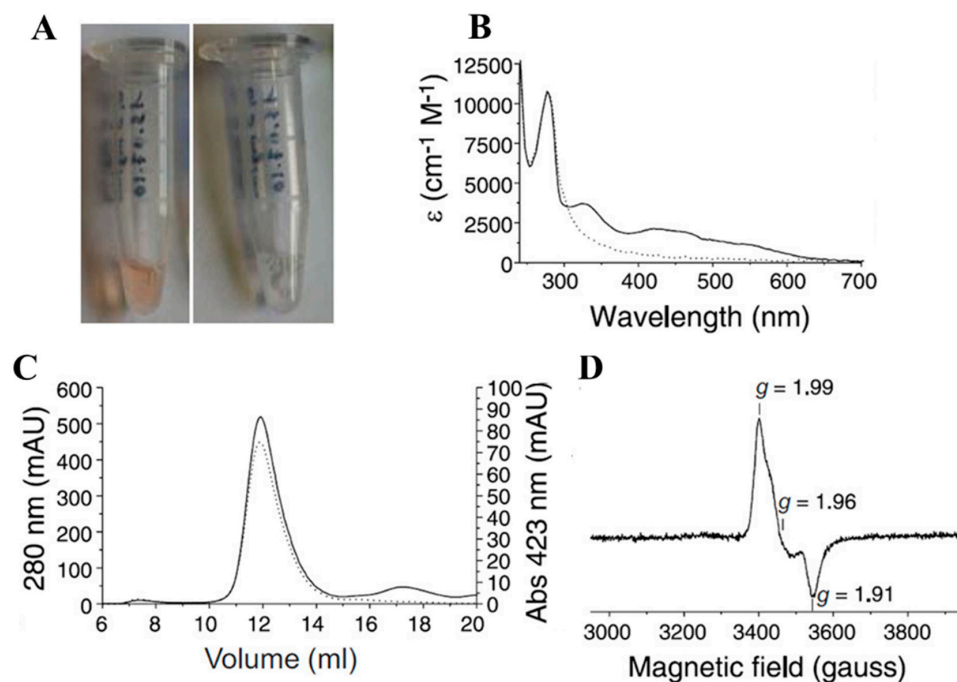


Figure 4. Characterization of a [2Fe-2S] cluster in nsp5 of Rotavirus. (A) Aerobically purified wild-type nsp5 (yellow) protein, become colorless when exposed to molecular oxygen overnight. (B) UV-vis spectra of purified nsp5 (solid line) and oxygen exposed sample (dotted line). (C) Size exclusion chromatography of nsp5 taken at 280 nm (solid line) and 423 nm (dotted line). (D) EPR spectrum of dithionite reduced nsp5 confirms the presence of a [2Fe-2S] cluster. Adopted from reference [60].

4.3. Tumor Antigen from Merkel Cell Polyomavirus (MCPyV) Consists of [Fe-S] Cluster

Polyomaviruses are common in a wide range of mammalian species, including humans [61]. Merkel cell polyomavirus (MCPyV), a significant portion of human cancer, is caused by among the five human polyomaviruses: JC, WU, KI, BK, and MCPyV. The early section of the MCPyV virus encodes both the large and small tumor (LT and sT, respectively) antigens necessary for the virus to proliferate in the human body. Since MCPyV sT is important in the viral life cycle, Tsang et al. investigated potential ways to hamper viral growth by targeting MCPyV sT protein [62]. When MCPyV sT was expressed and purified in *E. coli* in fusion with a maltose-binding protein (MBP), the cell pellet of the sT-gen was dark brown, a typical indicator of iron metal ions in the protein (Figure 5A). UV-Vis spectroscopic analysis showed peaks at 325 and 420 nm and a suppression of these peaks upon addition of sodium dithionite, indicating the presence of [Fe-S] cluster(s) (Figure 5B). To confirm it, EPR signals at different temperatures (12 and 40 K) supported the presence of two distinct [Fe-S] clusters, one [4Fe-4S]²⁺ and one [2Fe-2S]²⁺ cluster in MCPyV St (Figure 5C,D). Mutating the cluster coordinating cysteines eliminates its ability to stimulate viral DNA replication. Hence, these findings can be a new insight for possible drug targets for controlling MCPyV infection.

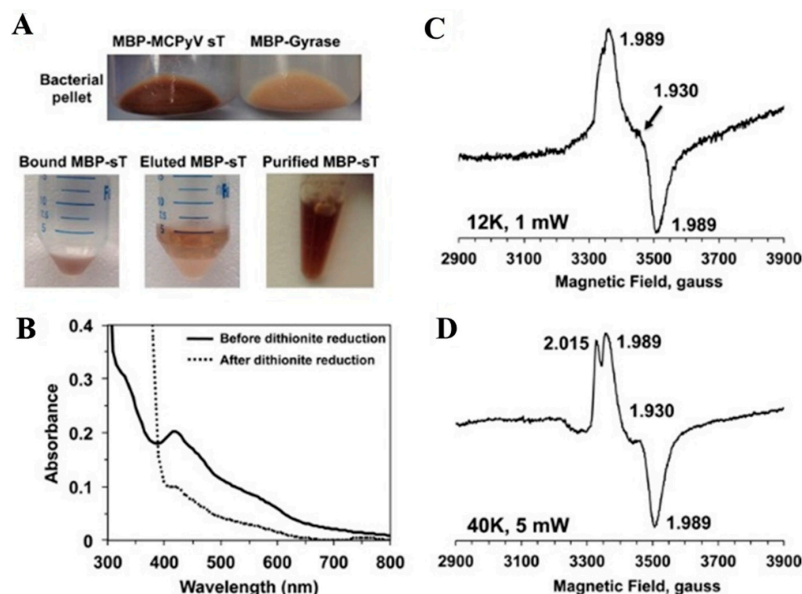


Figure 5. Identification of [Fe-S] cluster within the Merkel Cell Polyomavirus small T antigen (MCPyV sT). (A) The pure MBP-sT (dark brown) and cell pellet (dark brown) showed that the [Fe-S] cluster, a metal binding site, was occupied by MCPyV sT. (B) UV-vis spectra were obtained with dithionite present (dotted line) and absent (solid line). Excess sodium dithionite caused the distinctive band of the [Fe-S] cluster at 420 nm to vanish. (C) EPR spectrum was recorded before adding dithionite and (D) after adding 20 mM dithionite. Adopted from reference [62].

4.4. HBx—A [Fe-S] Cluster Containing Viral Replication Protein from Hepatitis B Virus (HBV)

In humans, hepatocytes are infected with the Hepatitis B Virus (HBV), leading to chronic infections and the development of hepatocellular carcinoma (HCC) [63]. HBV exhibits geographical variation and is classified into ten genotypes with common genes (P, C, S, and X) within seven viral proteins. Protein X (HBx) is pivotal in viral replication and contributes to hepatocarcinogenesis (HCC). Shi et al. purified MBP-HBx and observed a yellow-brown protein with an absorption peak at 415 nm, suggesting the presence of metal ions, potentially Zn, Fe and Cu [64]. Later, Pandelia et al. showed that HBx likely contains a [Fe-S] cluster, which can exist as either $[2\text{Fe-2S}]^{2+}$ or $[4\text{Fe-4S}]^{2+}$ clusters, depending on the purification condition (Figure 6) [21]. The aerobically purified HBx protein, which had a maltose-binding protein (MBP) or disulfide bond isomerase C (DsbC) as soluble tags, exhibited a reddish-brown color. UV-Vis bands at 325, 415, and 460 nm indicated the characteristics of a $[2\text{Fe-2S}]^{2+}$ cluster. On the other hand, optical characteristics at 420 nm were revealed by anaerobic purification, indicating the presence of a $[4\text{Fe-4S}]^{2+}$ cluster (Figure 6A), suggesting that the HBx [Fe-S] cluster is sensitive to molecular oxygen. Furthermore, when aerobically purified native samples were subjected to EPR after adding sodium dithionite, the g-values at 2.04, 1.94, and 1.94 demonstrated the characteristic signal of a $[4\text{Fe-4S}]^{1+}$ cluster instead of $[2\text{Fe-2S}]^{1+}$ clusters via reductive coupling mechanism (Figure 6B). Mössbauer analysis showed parameters of $[2\text{Fe-2S}]^{2+}$ cluster with quadrupole doublet ($\delta = 0.28$ mm/s, $\Delta E_Q = 0.51$ mm/s) for aerobically purified sample. In contrast, the anaerobic purified protein sample showed characteristics of $[4\text{Fe-4S}]^{2+}$ cluster with single quadrupole doublet ($\delta = 0.45$ mm/s and $\Delta E_Q = 1.11$ mm/s) (Figure 6C,D). Previously, it has been shown that the reductive coupling of two $[2\text{Fe-2S}]^{1+}$ clusters can form one $[4\text{Fe-4S}]^{2+}$ cluster. During this oxidative-reductive coupling process, degraded iron ($\text{Fe}^{3+}/\text{Fe}^{2+}$) features also appeared in the Mössbauer spectrum, suggesting that it might involve promoting carcinogenesis via Fenton chemistry (Figure 6E) [7,65,66]. These discoveries could help identify [Fe-S] clusters in viral proteins, offering new directions to understand how chronic HBV infection leads to cancerous outcomes.

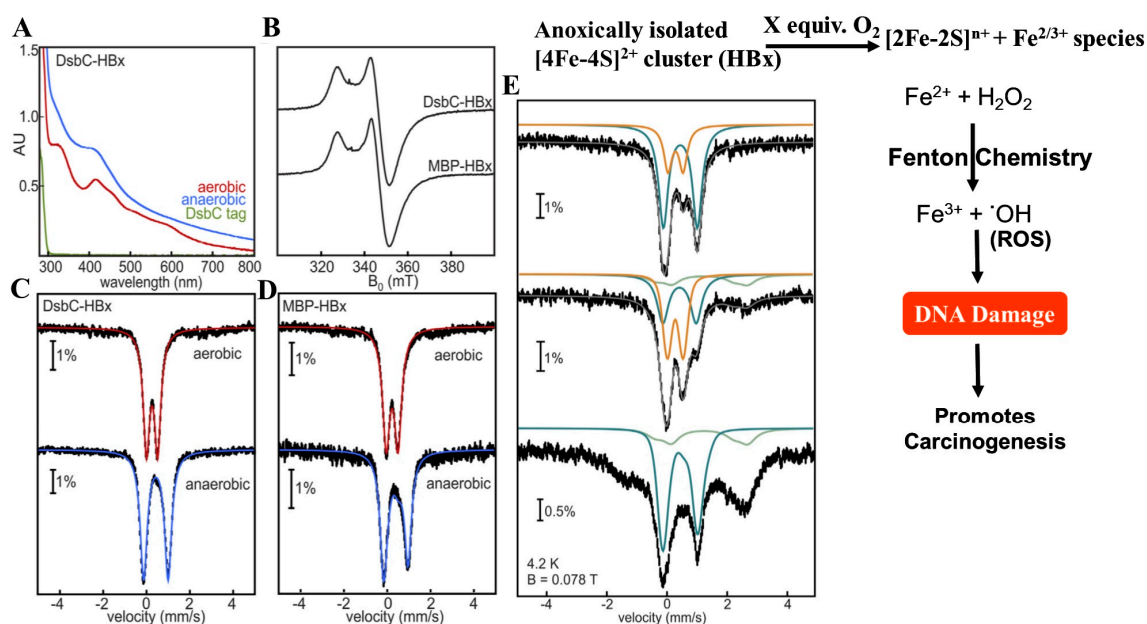


Figure 6. Characterization of the [Fe-S] cluster in the Hepatitis B Virus (HBV). (A) UV–visible spectra validated the existence of the $[4\text{Fe-4S}]^{2+}$ cluster under anaerobic purification conditions (blue line) and in the aerobic condition as $[2\text{Fe-2S}]^{2+}$ cluster (red line). At the same time, no band was observed for the DsbC tag (green line). (B) The EPR spectra of the DsbC and MBP–tagged HBx samples showed the presence of the $[4\text{Fe-4S}]^{2+}$ cluster upon exposure to dithionite. (C,D) The Mössbauer spectra of DsbC–HBx and MBP–HBx samples, obtained using aerobic (red line) and anaerobic (blue line), exhibit the $[2\text{Fe-2S}]^{2+}$ cluster and the $[4\text{Fe-4S}]^{2+}$ cluster, respectively. (E) Anoxically purified DsbC–HBx (top) after 4h of exposure to air (middle) and in the presence of excess sodium dithionite (bottom) [21]. All experimental Mössbauer spectrum (shown by vertical bars) were simulated (gray lines) using aggregated fits from individual subspectra (orange for $[2\text{Fe-2S}]$, teal for $[4\text{Fe-4S}]$, and light green for Fe^{2+}). Adopted from reference [7,21].

4.5. GciS—A Glycine and Cysteine Rich Protein from Mimivirus That Contains [Fe-S] Cluster

Giant DNA viruses that infect eukaryotes in various situations are known as giant viruses. In 2003, the first massive virus was identified as Mimivirus [67]. Villalta et al. recently identified a small protein, Glycine/Cysteine-rich Iron-Sulfur (GciS), in Mimivirus (Figure 7) [44]. However, its role is yet to be characterized. They found that when GciS was expressed in *E. coli* aerobically, the cell pellets were red in color. Inductively coupled plasma-mass spectrometry (ICP-MS) elemental analysis revealed that iron metal ions and optical characteristics in the GciS features in UV-Visible at 335, 418, 462, 513, and 586 nm suggested the presence of [Fe-S] cluster(s) (Figure 7A). The UV-Vis features at 330, 420, 460, and 550 nm are characteristic features of a $[2\text{Fe-2S}]$ cluster, and bands at 586 nm closer to 600 nm are probably the characteristics of a linear-type $[3\text{Fe-4S}]^{1+}$ cluster. Furthermore, the EPR spectrum is evident for the two different types of [Fe-S] clusters, predominantly a linear $[3\text{Fe-4S}]^{1+}$ cluster (paramagnetic with $S = 5/2$) and $[2\text{Fe-2S}]^{2+}$ cluster (Figure 7B). Finally, the Mössbauer analysis confirmed the presence of a paramagnetic linear $[3\text{Fe-4S}]^{1+}$ cluster and a $[2\text{Fe-2S}]^{2+}$ cluster (Figure 7C). The stability of the GciS protein was assessed following exposure to air, revealing that the spectral profile remained consistent before and after exposure. This observation indicates that molecular oxygen unaffected the [Fe-S] cluster's composition and nature during and after the protein purification process. Consequently, these glycine/cysteine-rich proteins form a novel class of viral [Fe-S] proteins with unique characteristics about [Fe-S] cluster binding. Investigating the [Fe-S] binding characteristics of GciS proteins in relation to their structural characteristics is essential. This work provides an essential precondition by providing information on their physiological significance with the potential of discovering novel roles related to viral [Fe-S] proteins.

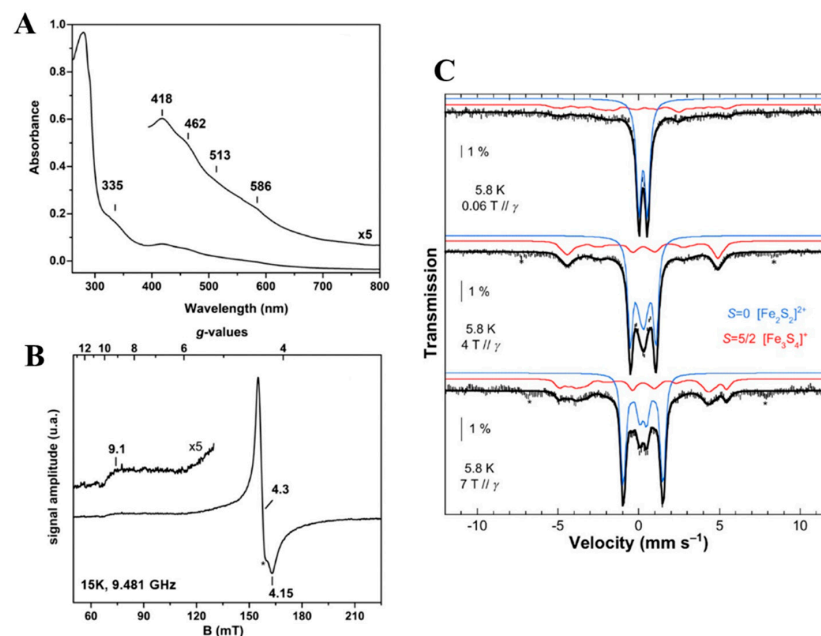


Figure 7. The mimivirus' [Fe-S] cluster identification. (A) A [2Fe-2S] cluster is characterized by its UV–Vis features at 330, 420, 460, and 550 nm. A linear-type [3Fe-4S]¹⁺ cluster is most likely represented by the bands at 586 nm that are closer to 600 nm. (B) Two distinct forms of [Fe-S] clusters as [2Fe-2S]²⁺ and [3Fe-4S]¹⁺ are visible in the EPR spectrum. (C) Mossbauer analysis confirmed the presence of [2Fe-2S]²⁺ and paramagnetic linear [3Fe-4S]¹⁺ cluster. Simulation is represented by black line, blue for [2Fe-2S], red for [3Fe-4S]¹⁺. Adopted from reference [44].

4.6. *Nsp12* and *nsp13*—A [Fe-S] Cluster Containing Protein That Regulates RNA Polymerase Activity in Coronaviruses

Coronaviruses constitute a diverse group of viruses that infect both humans and the respiratory system of many animals. Severe outbreaks of two highly virulent zoonotic coronaviruses, SARS-CoV and MERS-CoV, were detected in 2002 and 2012, causing respiratory system damage [68–70]. SARS-CoV-2, a new coronavirus, emerged in late 2019 in Wuhan, China, inducing atypical viral pneumonia in individuals. The structure of the viral protein (*nsp12*), which was determined by cryo-EM, clearly showed that two zinc metal ions were present and coordinated by three cysteine ligands and one histidine ligand [71]. Later, Maio et al. purified *nsp12* under anaerobic conditions, they discovered that the RdRp unit coordinates two [4Fe-4S]²⁺ clusters at locations initially believed to be Zn-bound (Figure 8) [22]. The optical features at 420 nm indicate the presence of [Fe-S] cluster(s) (Figure 8A). A single quadruple splitting ($\Delta E_Q = 1.25$ mm/s) with an isomeric shift ($\delta = 0.44$ mm/s), a distinguishing feature of a typical [4Fe-4S]²⁺ cluster unit, was observed in the 4.2 K Mössbauer spectrum (Figure 8B). Because wild-type *nsp12* bonded 7.5 ± 0.35 Fe atoms per monomer, they interpreted the Mössbauer spectrum as two [4Fe-4S]²⁺ clusters. X-band EPR study for purified *nsp12* [4Fe-4S]²⁺ showed silent EPR features; in the presence of sodium dithionite, a distinct signal for the [4Fe-4S]¹⁺ clusters appeared, confirming the presence of the [4Fe-4S] cluster in *nsp12* (Figure 8C). The [4Fe-4S] cluster-containing RdRp protein absorbance at 420 nm diminishes upon incubating with 4-hydroxy-2,2,6,6-tetramethylpiperidin-1-oxyl (TEMPO), a six-membered nitric oxide complex due to [Fe-S] cluster degradation (Figure 8E). Therefore, the [4Fe-4S]²⁺ clusters oxidized by TEMPO, which causes structural deterioration, may restrict RdRp activity, and hinder replication of SARS-CoV-2 in cell culture (Figure 8F).

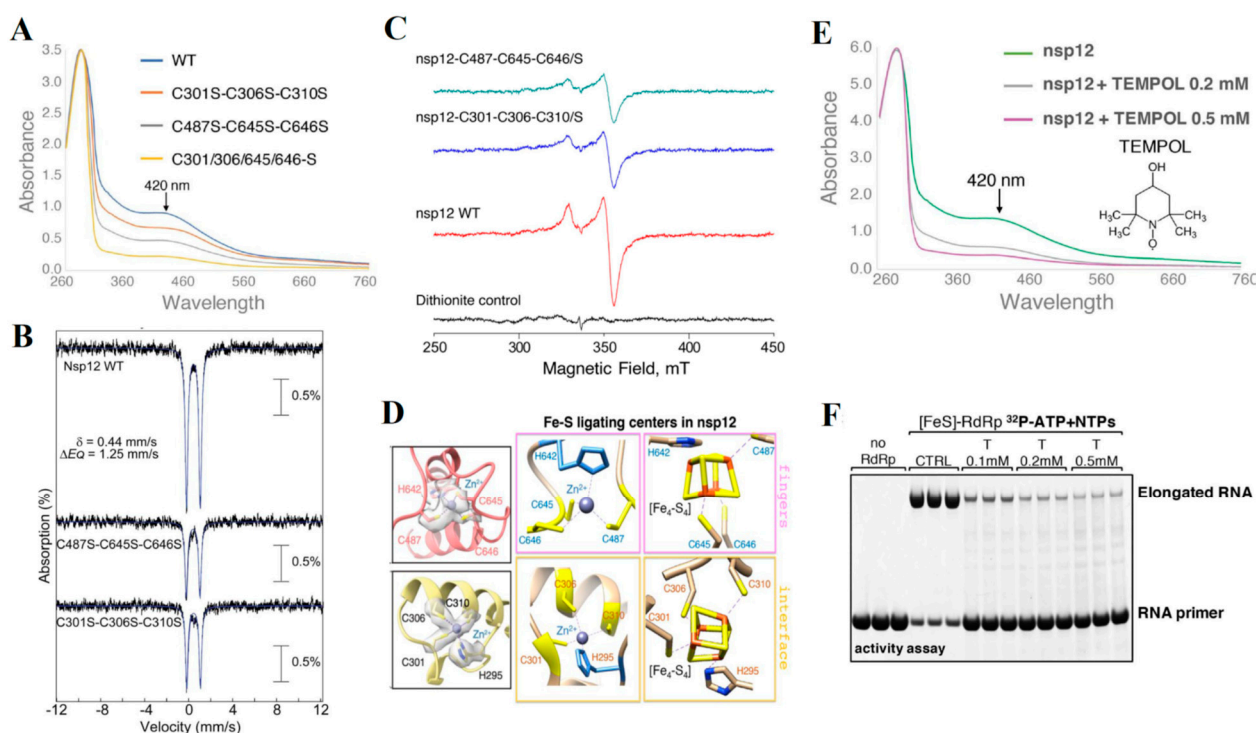


Figure 8. Discovery of $[4\text{Fe-4S}]^{2+}$ clusters in SARS-CoV-2 nsp12. (A) The UV-visible band at 420 nm indicates the presence of the $[4\text{Fe-4S}]^{2+}$ clusters in nsp12 (WT or variants) with two metal-ligand binding sites. (B) Mössbauer spectra of nsp12 (WT and variants) showed parameters of a quadrupole doublet typical of $[4\text{Fe-4S}]^{2+}$ cluster with ~95% cluster occupancy. (C) After reduction with sodium dithionite, EPR studies of nsp12 samples reveal $[4\text{Fe-4S}]^{2+}$ clusters. (D) The potential $[\text{Fe-S}]$ ligating sites are depicted in the ribbon mode of the catalytic subunit, nsp12. (E) UV-vis spectra of anoxically purified nsp12 before and after in vivo TEMPOL treatment showing disintegration of $[4\text{Fe-4S}]^{2+}$ cluster. (F) Activity assay shows increased TEMPOL concentration, leading to diminished RNA polymerase activity. Adopted from reference [22,23].

Recently, the same group discovered that nsp13 harbors a $[4\text{Fe-4S}]^{2+}$ cluster in its zinc-binding domain (ZBD) (Figure 9) [23]. The anoxically purified nsp13 sample showed a UV-visible band at ~420 nm, indicating the presence of a $[4\text{Fe-4S}]^{2+}$ cluster (Figure 9A). The ^{57}Fe -rich nsp13 sample was subjected to Mössbauer analysis, featuring the parameters of a quadrupole doublet typical of $[4\text{Fe-4S}]^{2+}$ cluster [$\delta = 0.44 \text{ mm/s}$, $\Delta E_Q = 1.24 \text{ mm/s}$] along with a minor quadrupole doublet of $[2\text{Fe-2S}]^{2+}$ cluster ($\delta = 0.30 \text{ mm/s}$, $\Delta E_Q = 0.42 \text{ mm/s}$) (Figure 9B). In the presence of dithionite, the anoxic purified sample showed an EPR feature of a reduced $[4\text{Fe-4S}]^{1+}$ cluster with g-values of 2.05, 1.92, and 1.86 (Figure 9C). The ICP-MS analysis for 3.6 ± 0.1 Fe ions and 2 ± 0.2 Zn ions per protomer bound to helicase nsp13 (Figure 9D). The biochemical studies showed that the $[4\text{Fe-4S}]^{2+}$ cluster containing nsp13 binds more tightly and modulates the helicase's unwinding activity. The addition of TEMPOL disintegrates the $[4\text{Fe-4S}]^{2+}$ cluster, hence inhibiting its unwinding ability (Figure 9E). The results from both these research studies showed that TEMPOL, operating through a unique mechanism compared to other antivirals, could serve as a potential low-toxicity oral option for preventing SARS-CoV-2 after exposure. These research findings will provide brand-new treatment targets for many RNA and DNA viruses.

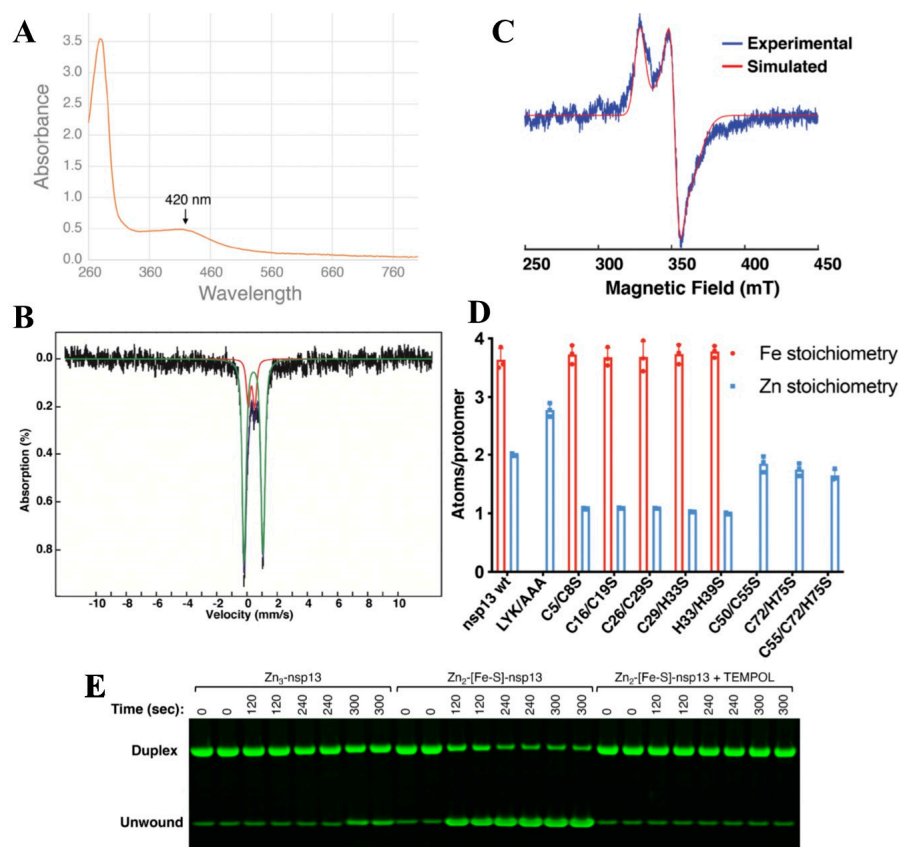


Figure 9. Characterization of helicase nsp13 of SARS–CoV–2 containing $[4\text{Fe-4S}]^{2+}$ cluster. (A) UV–Vis feature at 420 nm confirms the presence of a $[4\text{Fe-4S}]^{2+}$ cluster. (B) Mössbauer analysis of ^{57}Fe rich nsp13 sample showed a single quadrupole doublet typical of $[4\text{Fe-4S}]^{2+}$ cluster (green line), with a minor quadrupole doublet of $[2\text{Fe-2S}]^{2+}$ cluster (red line). (C) The EPR spectrum of anaerobically purified nsp13 in the presence of dithionite confirms the presence of predominantly a $[4\text{Fe-4S}]^{1+}$ cluster. (D) The stoichiometry analysis showed 3.6 ± 0.1 Fe ions and 2 ± 0.2 Zn ions per protomer bound to helicase nsp13. (E) The unwinding activity of nsp13 gets hindered upon TEMPOL treatment because it disintegrates the $[4\text{Fe-4S}]^{2+}$ cluster. Adopted from reference [23].

5. [Fe-S] Clusters Functions in Pathogenic Bacteria

With widespread overuse of antibiotics, there has been a surge in the emergence of drug resistant bacterial pathogens in recent times. The most well-known subset are the ESKAPE pathogens that comprise of *Enterococcus faecium*, *Staphylococcus aureus*, *Klebsiella pneumoniae*, *Acinetobacter baumannii*, *Pseudomonas aeruginosa*, and *Enterobacter* spp. Other examples include multidrug resistant tuberculosis (MDR TB) and Methicillin-resistant *Staphylococcus aureus* (MRSA). These have led to the need to develop new antibiotics and different drug targets. Characterizing [Fe-S] cluster containing proteins that are essential for the pathogens can open up new avenues for diagnostics and therapeutics [72].

5.1. WhiB3—A Fe-S Cluster Containing Transcriptional Regulator from M Tuberculosis

WhiB-like proteins are a family of transcription factors that are found exclusively in Actinobacteria [73]. They have a $[4\text{Fe-4S}]$ iron-sulfur cluster and play important roles ranging from antibiotic resistance, pathogenesis and cell development [9,74]. *Mycobacterium tuberculosis* WhiB3 plays a crucial role in its survival and pathogenesis. *Mt* WhiB3 binds to the conserved region 4 of principal sigma factor (σ^A_4). Recently, Tao et al. solved the crystal structure of WhiB3: σ^A_4 complex without and with DNA (Figure 10) [75]. The binding interface between the WhiB3 and σ^A_4 is in close proximity to the $[4\text{Fe-4S}]$ cluster. WhiB3's conserved aromatic residues near the $[4\text{Fe-4S}]$ namely F31, F32 and W76 drive the

complex formation between WhiB3 and σ^A_4 (Figure 10A,B). Single alanine mutations on these residues prevented complex formation that was validated by pull down assays. These findings show that the [Fe-S] cluster could be playing an important role in the proper folding of *Mt* WhiB3. In case of σ^A_4 , mutating H516 to an alanine prevents the complex formation. Using a *pk3* promoter, which is involved in the biosynthesis of complex polyketides in *Mt* as the DNA template for a binding study, Tao et al. showed that the C-terminal residues from 91–102 of WhiB3 are essential for DNA binding using electrophoretic mobility shift assays (EMSA) (Figure 10E,F). Crystal structure of WhiB3: σ^A_4 - β_{tip} in complex with WhiB7 promoter DNA P_{whiB7} identified an arginine-rich motif (R38, R40 and R42) in WhiB3 that might be playing a crucial role in DNA binding (Figure 10C,D). A triple arginine to alanine mutation of the arginine motif abolishes DNA binding in EMSA strengthening the structural analysis. These structural insights into the WhiB family of proteins will potentially open up new drug targets for tuberculosis treatment.

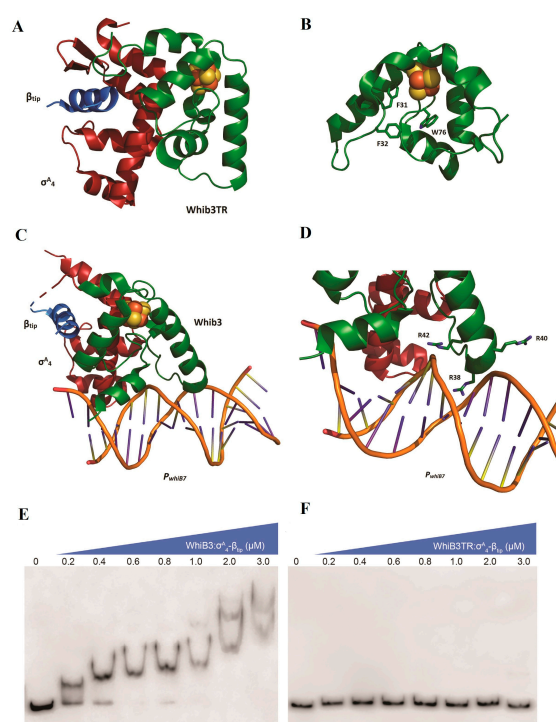


Figure 10. (A) Crystal structure of truncated WhiB3: σ^A_4 - β_{tip} complex with β_{tip} from the neighboring complex interacting with σ^A_4 and WhiB3 (PDB ID: 8CWR). (B) Aromatic residues in WhiB3 which are important for complex formation (PDB ID: 8CWR). (C) Crystal structure of WhiB3: σ^A_4 - β_{tip} in complex with WhiB7 promoter DNA P_{whiB7} (PDB ID: 8CYF). (D) Conserved Arginine-rich DNA binding motif in WhiB3 (PDB ID: 8CYF). (E,F), EMSAs of the WhiB3: σ^A_4 - β_{tip} complex with *pk3* promoter, (E) with wildtype WhiB3 protein and (F) with the truncated WhiB3 (WhiB3TR) lacking the C-terminal residues 91 to 102. Adopted from reference [75].

5.2. Ferric Uptake Regulators (*Fur*): A Transcription Factor That Regulates Intracellular Iron Homeostasis

Fur is a transcription factor that utilizes Fe^{2+} as a corepressor and represses siderophore synthesis in pathogens [76,77]. Previous attempts to purify iron-bound *Fur* from bacteria were unsuccessful. Recent studies by Chelsey et al. have shown that *Fur* from *Escherichia coli*, *Haemophilus influenzae*, *Vibrio cholerae*, and *Helicobacter pylori* binds a [2Fe-2S] cluster via the conserved cysteine residues when expressed in the *E. coli* mutant cells with elevated intracellular free iron [78]. Knocking out the iron-sulfur cluster assembly proteins *IscA* and *SufA* elevated the intracellular free iron levels, which was confirmed by EPR. Knocking out *IscA* and *SufA* in *E. coli* cells has minor or no effect on [2Fe-2S] cluster assembly. *Ec Fur* expressed in the *E. coli iscA/sufA* mutant cells primarily bound a novel [2Fe-2S]

cluster which was confirmed by UV-visible spectroscopy, Mössbauer spectroscopy, and EPR (Figure 11A–C). [2Fe-2S] cluster have UV-Vis spectroscopic features around 325 nm, 410 nm, and 450 nm. Site-directed mutagenetic studies identified the conserved cysteine residues C93, C96, and C133 as the ligands for the [2Fe-2S] cluster (Figure 11D). The fourth cysteine residue C138 is not conserved. Mutation studies reported by Chelsey et al. on C138 were inconclusive. Purifying the C138A variant was unsuccessful, and the C138S variant could bind a [2Fe-2S] cluster. The UV-Vis spectrum of the C138S variant showed subtle differences compared to the wild type but was not as significant as the conserved cysteine residue variants. The occupancy of the cluster was around 31% when *Ec* Fur was expressed in *E. coli iscA/sufA* mutant cells. It dropped to 4% when expressed in *E. coli* wt cells, strengthening the current hypothesis that *Ec* Fur binds to [2Fe-2S] cluster reversibly depending on the intracellular free iron levels. It is proposed that [2Fe-2S] bound Fur performs the role of an active repressor throttling down siderophore synthesis at high iron levels and apo Fur is an inactive repressor at low iron levels upregulating siderophore synthesis. Chelsey et al. also claimed that the occupancy of [2Fe-2S] cluster varies among different species. They correlate the occupancy to the binding affinity. Among the Fur proteins expressed in *E. coli*, *Hi* Fur had the highest occupancy for the [2Fe-2S] cluster, followed by *Ec* Fur (Figure 11E,F). This has to be investigated further since the difference in occupancy can also be due to some Furs expressing well over the other in *E. coli*. Nevertheless, this also potentially indicates that Fur proteins from different species activate at different intracellular iron levels that can come in handy during drug discovery.

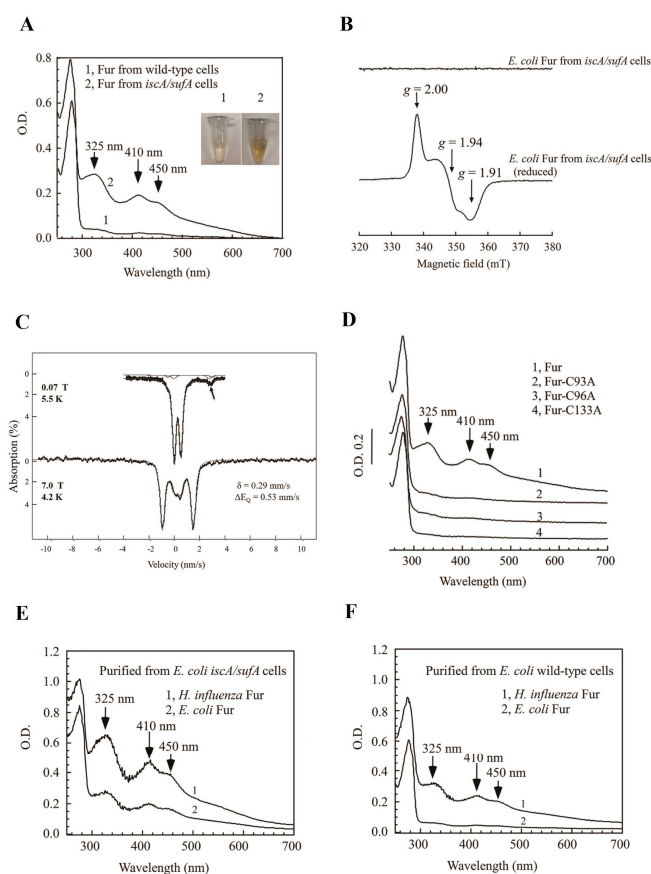


Figure 11. (A) UV–Vis spectrum of *Ec* Fur expressed in the *Ec* wt and *Ec iscA/sufA* mutant cells. (B) EPR spectra of *Ec* Fur protein purified from the *iscA/sufA* mutant cells. (C) Mössbauer spectra of the ^{57}Fe -enriched *Ec* Fur from the *iscA/sufA* mutant cells. (D) UV–Vis spectrum of *Ec* Fur wt and cluster coordinating cysteine mutants. (E) UV–Vis spectrum of *Hi* Fur and *Ec* Fur purified from *Ec iscA/sufA* mutant cells. (F) UV–Vis spectrum of *Hi* Fur and *Ec* Fur purified from *Ec* wt cells. Adopted from reference [78].

5.3. Ferrous Iron Transport Protein C (FeoC): A Fe-S Cluster Containing Protein That Regulates the Ferrous Iron Channel

The Feo system is composed of three proteins: a main membrane protein (FeoB) essential for iron translocation and two small cytosolic proteins (FeoA and FeoC), hypothesized to function as accessories to this process [79]. Bacteria have evolved many types of iron acquisition systems to maintain iron levels within the cell. In anaerobic conditions, ferrous iron (Fe^{2+}) is more abundant [80]. Therefore, for bacteria to survive under oxygen limiting conditions, ferrous iron uptake pathways are essential. Previous studies have implicated the Feo system for the virulence in pathogens such as *Helicobacter pylori*, *Pseudomonas aeruginosa* [81]. In 2013, Kuang et al. reported that under anaerobic conditions, *Klebsiella pneumoniae* FeoC bound a [4Fe-4S] cluster using UV-Visible spectroscopy, EPR, and X-ray absorption methods (Figure 12A–E) [82]. Native *Kp* FeoC EPR showed characteristics of a [4Fe-4S] $^{3+}$ cluster (Figure 12A). Exposing [4Fe-4S] cluster bound *Kp* FeoC to oxygen lead to the breakdown of cluster and loss of characteristic absorption peaks. Solution structures of FeoC from *K. pneumoniae* and *E. coli* have a disordered wing loop1 (W1), containing four conserved Cys residues in a sequence, CX₄CX₂CX_{5,8}C (Figure 12H) [83]. Site-directed mutagenesis on those cysteines confirmed that they are the ligands for the [4Fe-4S] cluster. In 2022, Kuang et al. reported that the iron-sulfur cluster of *Kp* FeoC increased the GTPase rate of *Kp* N-terminal domain FeoB (NFeoB). The presence of 7% FeoC [4Fe-4S] $^{3+}$ enhanced the GTPase rate of NFeoB by 3.6-fold. When the cluster was reduced to 7% FeoC [4Fe-4S] $^{2+}$ using DTT, the rate of enhancement dropped to 1.7-fold (Figure 12F,G). With apo FeoC, the rate of enhancement was 1.6-fold. This suggested that [4Fe-4S] $^{3+}$ is the active form and [4Fe-4S] $^{2+}$ is the inactive form.

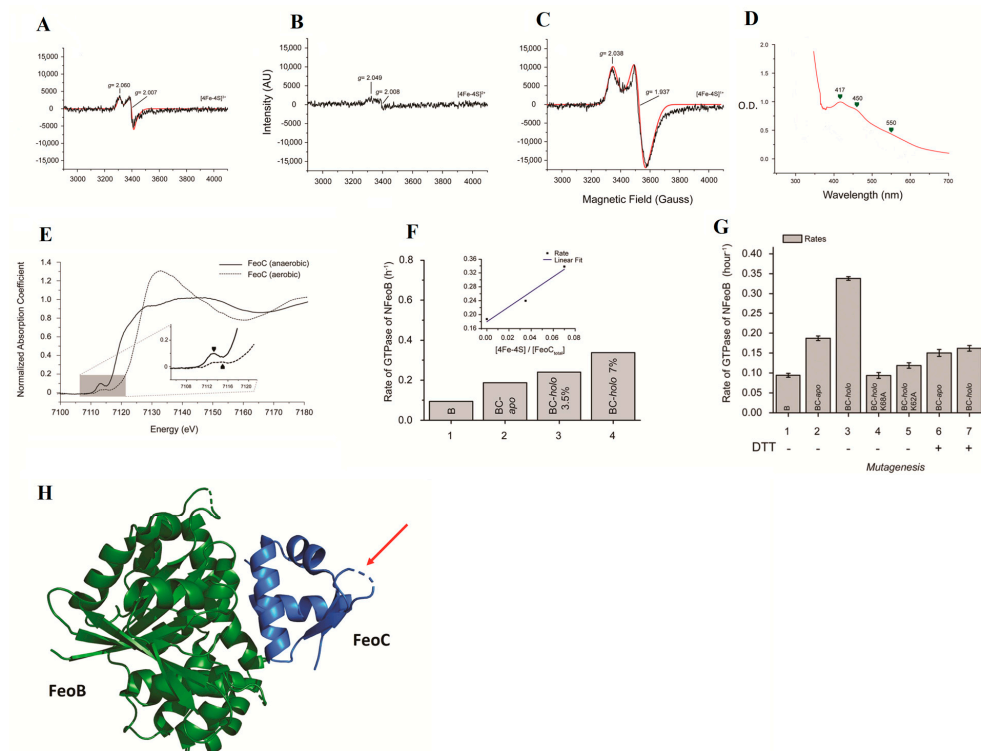


Figure 12. EPR spectrum of *Kp* FeoC at different redox states. (A) Native state. (B) DTT–reduced state. (C) Fully reduced by sodium dithionite. (D) UV–Vis spectrum of *Kp* FeoC. (E) X–ray absorption spectrum of *holo*–FeoC at the Fe K–edge. (F) Effect of various forms of FeoC on the GTPase rate of NFeoB. (G) GTPase activity of NFeoB in the presence of FeoC K62A and K68A (Lane 4 and 5). GTPase activity in the presence of DTT (Lane 6 and 7). (H) Crystal structure of *K. pneumoniae* NFeoBC complex (PDB ID: 7WQU). The loop containing the ligands for the [Fe–S] cluster are missing and disordered in the structure, pointed by the red arrow. Adopted from reference [82,83].

When positively charged amino acids K62 and K68 close to the $[4\text{Fe-4S}]^{3+}$ cluster in FeoC were mutated to alanine, it led to a reduced enhancement of GTPase activity in NFeoB: K62A (from 3.6- to 1.3-fold); K68A (from 3.6- to 1.0-fold) showing the importance of these residues in NFeoB GTPase activity (Figure 12G). These studies reveal that the [Fe-S] cluster of FeoC and its oxidation state regulates GTPase activity. Crystal structure of NFeoBC complex suggested residue T37 of NFeoB is involved in catalysis. Mutating it to a serine reduced the NFeoB activity by 87%, validating the hypothesis. $[4\text{Fe-4S}]^{3+}$ cluster along with residues K62 and K68 in FeoC and residue T37 in NFeoB could be playing an important role in electron transfer affecting NFeoB's GTPase activity thereby impacting how bacteria deal with oxidative stress. FeoC can potentially be a good drug target in *Klebsiella pneumoniae*.

6. Conclusions and Future Perspectives

In this review article, we highlight the critical roles of iron-sulfur cluster-containing enzymes in pathogens. The understanding of [Fe-S] clusters in human health, such as cancer, neurodegenerative diseases, and iron homeostasis, has grown over the years. Due to oxygen sensitivity and logistical issues, the characterization of [Fe-S] cluster-containing enzymes, in general, and their potential as new drug targets remains challenging. Iron (Fe) and zinc (Zn) ions have comparable chemical functions but differ in reactivity and functionality. This difference arises mainly because Fe is redox-active and oxygen-sensitive, while Zn is redox-inert and tolerant towards oxygen. In many cases, Fe, Zn also provides structural stability and functionality in various metalloproteins. Furthermore, Zn mainly displays tetrahedral coordination unlike other metal ions, such as redox-active copper or Fe, under aerobic conditions. As a result, wide ranges of metalloproteins were previously annotated as zinc finger proteins. Advanced spectroscopic techniques and improved biochemical assays and structural techniques have revealed the presence of [Fe-S] clusters, including eukaryotic MitoNEET protein, regulatory proteins like iron-sensing transcriptional repressor (Fep1), and viral proteins like oncogenic small tumor antigen of the Merkel Cell Polyomavirus (MCPyV), hepatitis b (HBx), SARS-CoV-2 nonstructural proteins (nsp12, nsp13). The biophysical, biochemical, and electrochemical characterization techniques discussed in this review will be essential for identifying and characterizing unexplored enzymes containing [Fe-S] clusters in the future. Despite these preliminary findings, the function of [Fe-S] clusters in infectious diseases remains elusive. Future research efforts are anticipated to help fill this gap, and characterizing [Fe-S] cluster proteins in pathogens will open up new avenues for diagnostics and therapeutics.

Author Contributions: Conceptualization, M.K.R.; investigation, M.K.R. and V.R.J.; writing—original draft preparation, M.K.R., V.R.J. and S.B.; writing—review and editing, M.K.R., V.R.J. and S.B.; supervision, M.K.R. All authors have read and agreed to the published version of the manuscript.

Funding: This research received no external funding.

Acknowledgments: M.K.R. is grateful for support from J.M.B Jr., C. K. and the Eberly Research Fellows Program.

Conflicts of Interest: The authors declare no conflicts of interest.

References

1. Garcia, P.S.; D'Angelo, F.; Ollagnier de Choudens, S.; Dussouchaud, M.; Bouveret, E.; Gribaldo, S.; Barras, F. An Early Origin of Iron-Sulfur Cluster Biosynthesis Machineries before Earth Oxygenation. *Nat. Ecol. Evol.* **2022**, *6*, 1564–1572. [[CrossRef](#)] [[PubMed](#)]
2. Johnson, D.C.; Dean, D.R.; Smith, A.D.; Johnson, M.K. Structure, function, and formation of biological iron-sulfur clusters. *Annu. Rev. Biochem.* **2005**, *74*, 247–281. [[CrossRef](#)]
3. Beinert, H.; Holm, R.H.; Münck, E. Iron-Sulfur Clusters: Nature's Modular, Multipurpose Structures. *Science* **1997**, *277*, 653–659. [[CrossRef](#)] [[PubMed](#)]
4. Schulz, V.; Basu, S.; Freibert, S.A.; Webert, H.; Boss, L.; Mühlhoff, U.; Pierrel, F.; Essen, L.O.; Warui, D.M.; Booker, S.J.; et al. Functional spectrum and specificity of mitochondrial ferredoxins FDX1 and FDX2. *Nat. Chem. Biol.* **2023**, *19*, 206–217. [[CrossRef](#)] [[PubMed](#)]

5. Khodour, Y.; Kaguni, L.S.; Stiban, J. Iron-sulfur clusters in nucleic acid metabolism: Varying roles of ancient cofactors. *Enzymes* **2019**, *45*, 225–256. [[PubMed](#)]
6. Rouault, T.A.; Tong, W.H. Iron-sulfur cluster biogenesis and human disease. *Trends Genet.* **2008**, *24*, 398–407. [[CrossRef](#)] [[PubMed](#)]
7. Raza, M.K.; Karges, J. Iron-Sulfur Clusters in Viral Diseases. In *Encyclopedia of Inorganic and Bioinorganic Chemistry*; Scott, R.A., Ed.; Wiley: Hoboken, NJ, USA, 2024. [[CrossRef](#)]
8. Honarmand, E.K.; Ciofi-Baffoni, S.; Hagedoorn, P.L.; Nicolet, Y.; Le Brun, N.E.; Hagen, W.R.; Armstrong, F.A. Iron-sulfur clusters as inhibitors and catalysts of viral replication. *Nat. Chem.* **2022**, *14*, 253–266. [[CrossRef](#)]
9. Elchennawi, I.; Ollagnier de Choudens, S. Iron-Sulfur Clusters toward Stresses: Implication for Understanding and Fighting Tuberculosis. *Inorganics* **2022**, *10*, 174. [[CrossRef](#)]
10. Fuss, J.O.; Tsai, C.-L.; Ishida, J.P.; Tainer, J.A. Emerging critical roles of Fe-S clusters in DNA replication and repair. *Biochim. Biophys. Acta* **2015**, *1853*, 1253–1271. [[CrossRef](#)]
11. Barton, J.K.; Silva, R.M.B.; O'Brien, E. Redox Chemistry in the Genome: Emergence of the [4Fe4S] Cofactor in Repair and Replication. *Annu. Rev. Biochem.* **2019**, *88*, 163–190. [[CrossRef](#)]
12. Boal, A.K.; Genereux, J.C.; Sontz, P.A.; Gralnick, J.A.; Newman, D.K.; Barton, J.K. Redox signaling between DNA repair proteins for efficient lesion detection. *Proc. Natl. Acad. Sci. USA* **2009**, *106*, 15237–15342. [[CrossRef](#)] [[PubMed](#)]
13. Pinto, M.N.; Ter Beek, J.; Ekanger, L.A.; Johansson, E.; Barton, J.K. The [4Fe4S] cluster of yeast DNA polymerase ϵ is redox active and can undergo DNA-mediated signaling. *J. Am. Chem. Soc.* **2021**, *143*, 16147–16153. [[CrossRef](#)] [[PubMed](#)]
14. O'Brien, E.; Holt, M.E.; Thompson, M.K.; Salay, L.E.; Ehlinger, A.C.; Chazin, W.J.; Barton, J.K. The [4Fe4S] cluster of human DNA primase functions as a redox switch using DNA charge transport. *Science* **2017**, *355*, eaag1789. [[CrossRef](#)] [[PubMed](#)]
15. Salay, L.E.; Blee, A.M.; Raza, M.K.; Gallagher, K.S.; Chen, H.; Dorfeuille, A.J.; Barton, J.K.; Chazin, W.J. Modification of the 4Fe-4S Cluster Charge Transport Pathway Alters RNA Synthesis by Yeast DNA Primase. *Biochemistry* **2022**, *61*, 1113–1123. [[CrossRef](#)] [[PubMed](#)]
16. Imlay, J.A. Iron-sulphur clusters and the problem with oxygen. *Mol. Microbiol.* **2006**, *59*, 1073–1082. [[CrossRef](#)]
17. Pritts, J.D.; Michel, S.L.J. Fe-S clusters masquerading as zinc finger proteins. *J. Inorg. Biochem.* **2022**, *230*, 111756. [[CrossRef](#)] [[PubMed](#)]
18. Chen, J.; Calderone, L.A.; Pan, L.; Quist, T.; Pandelia, M.-E. The Fe and Zn cofactor dilemma. *Biochim. Biophys. Acta-Proteins Proteom.* **2023**, *1871*, 140931.
19. Wiley, S.E.; Paddock, M.L.; Abresch, E.C.; Gross, L.; van der Geer, P.; Nechushtai, R.; Murphy, A.N.; Jennings, P.A.; Dixon, J.E. The outer mitochondrial membrane protein mitoNEET contains a novel redox-active 2Fe-2S cluster. *J. Biol. Chem.* **2007**, *282*, 23745–23749. [[CrossRef](#)]
20. Ye, H.; Rouault, T.A. Human iron-sulfur cluster assembly, cellular iron homeostasis, and disease. *Biochemistry* **2010**, *49*, 4945–4956. [[CrossRef](#)]
21. Ueda, C.; Langton, M.; Chen, J.; Pandelia, M.E. The HBx protein from hepatitis B virus coordinates a redox-active Fe-S cluster. *J. Biol. Chem.* **2022**, *298*, 101698. [[CrossRef](#)]
22. Maio, N.; Lafont, B.A.P.; Sil, D.; Li, Y.; Bollinger, J.M., Jr.; Krebs, C.; Pierson, T.C.; Linehan, W.M.; Rouault, T.A. Fe-S cofactors in the SARS-CoV-2 RNA-dependent RNA polymerase are potential antiviral targets. *Science* **2021**, *373*, 236–241. [[CrossRef](#)]
23. Maio, N.; Raza, M.K.; Li, Y.; Zhang, D.L.; Bollinger, J.M., Jr.; Krebs, C.; Rouault, T.A. An iron-sulfur cluster in the zinc-binding domain of the SARS-CoV-2 helicase modulates its RNA-binding and -unwinding activities. *Proc. Natl. Acad. Sci. USA* **2023**, *120*, e2303860120. [[CrossRef](#)]
24. Pain, D.; Dancis, A. Roles of Fe-S proteins: From cofactor synthesis to iron homeostasis to protein synthesis. *Curr. Opin. Genet. Dev.* **2016**, *38*, 45–51. [[CrossRef](#)] [[PubMed](#)]
25. Schulz, V.; Freibert, S.A.; Boss, L.; Mühlenhoff, U.; Stehling, O.; Lill, R. Mitochondrial [2Fe-2S] ferredoxins: New functions for old dogs. *FEBS Lett.* **2023**, *597*, 102–121. [[CrossRef](#)] [[PubMed](#)]
26. Hudson, J.M.; Heffron, K.; Kotlyar, V.; Sher, Y.; Maklashina, E.; Cecchini, G.; Armstrong, F.A. Electron transfer and catalytic control by the iron-sulfur clusters in a respiratory enzyme, *E. coli* fumarate reductase. *J. Am. Chem. Soc.* **2005**, *127*, 6977–6989. [[CrossRef](#)] [[PubMed](#)]
27. Castro, L.; Tórtora, V.; Mansilla, S.; Radi, R. Aconitases: Non-Redox Iron-Sulfur Proteins Sensitive to Reactive Species. *Acc. Chem. Res.* **2019**, *52*, 2609–2619. [[CrossRef](#)] [[PubMed](#)]
28. Lushchak, O.V.; Piroddi, M.; Galli, F.; Lushchak, V.I. Aconitase post-translational modification as a key in linkage between Krebs cycle, iron homeostasis, redox signaling, and metabolism of reactive oxygen species. *Redox Rep.* **2014**, *19*, 8–15. [[CrossRef](#)]
29. Broderick, J.B.; Duffus, B.R.; Duschene, K.S.; Shepard, E.M. Radical S-adenosylmethionine enzymes. *Chem. Rev.* **2014**, *114*, 4229–4317. [[CrossRef](#)]
30. Pandelia, M.E.; Lanz, N.D.; Booker, S.J.; Krebs, C. Mössbauer spectroscopy of Fe/S proteins. *Biochim Biophys Acta.* **2015**, *1853*, 1395–1405. [[CrossRef](#)]
31. Ueda, C.; Langton, M.; Pandelia, M.E. Characterization of Fe-S Clusters in Proteins by Mössbauer Spectroscopy. *Methods Mol. Biol.* **2021**, *2353*, 281–305.
32. Valer, L.; Rossetto, D.; Scintilla, S.; Hu, Y.J.; Tomar, A.; Nader, S.; Betinol, I.O.; Mansy, S.S. Methods to identify and characterize iron-sulfur oligopeptides in water. *Can. J. Chem.* **2022**, *100*, 475–483. [[CrossRef](#)]

33. Camponeschi, F.; Piccioli, M.; Banci, L. The Intriguing mitoNEET: Functional and Spectroscopic Properties of a Unique [2Fe-2S] Cluster Coordination Geometry. *Molecules* **2022**, *27*, 8218. [[CrossRef](#)] [[PubMed](#)]
34. Kennedy, M.C.; Kent, T.; Emptage, M.; Merkle, H.; Beinert, H.; Münck, E. Evidence for the formation of a linear [3Fe-4S] cluster in partially unfolded aconitase. *J. Biol. Chem.* **1984**, *259*, 14463–14471. [[CrossRef](#)] [[PubMed](#)]
35. Crack, J.C.; Le Brun, N.E. Native Mass Spectrometry of Iron-Sulfur Proteins. *Methods Mol. Biol.* **2021**, *2353*, 231–258. [[PubMed](#)]
36. Cai, K.; Markley, J.L. NMR as a Tool to Investigate the Processes of Mitochondrial and Cytosolic Iron-Sulfur Cluster Biosynthesis. *Molecules* **2018**, *23*, 2213. [[CrossRef](#)] [[PubMed](#)]
37. Banci, L.; Camponeschi, F.; Ciofi-Baffoni, S.; Piccioli, M. The NMR contribution to protein-protein networking in Fe-S protein maturation. *J. Biol. Inorg. Chem.* **2018**, *23*, 665–685. [[CrossRef](#)] [[PubMed](#)]
38. Tsai, C.L.; Tainer, J.A. Robust Production, Crystallization, Structure Determination, and Analysis of [Fe-S] Proteins: Uncovering Control of Electron Shuttling and Gating in the Respiratory Metabolism of Molybdopterin Guanine Dinucleotide Enzymes. *Methods Enzymol.* **2018**, *599*, 157–196. [[PubMed](#)]
39. Booker, S.J.; Lloyd, C.T. Twenty Years of Radical SAM! The Genesis of the Superfamily. *ACS Bio Med Chem Au* **2022**, *2*, 538–547. [[CrossRef](#)] [[PubMed](#)]
40. McLaughlin, M.I.; Lanz, N.D.; Goldman, P.J.; Lee, K.-H.; Booker, S.J.; Drennan, C.L. Crystallographic Snapshots of Sulfur Insertion by Lipoyl Synthase. *Proc. Natl. Acad. Sci. USA* **2016**, *113*, 9446–9450. [[CrossRef](#)]
41. Jeyachandran, V.R.; Pendyala, J.V.; McCarthy, E.L.; Boal, A.K.; Booker, S.J. Biochemical Approaches to Probe the Role of the Auxiliary Iron-Sulfur Cluster of Lipoyl Synthase from Mycobacterium Tuberculosis. *Methods Mol. Biol.* **2021**, *2353*, 307–332.
42. Stich, T.A. Characterization of Paramagnetic Iron-Sulfur Clusters Using Electron Paramagnetic Resonance Spectroscopy. *Methods Mol. Biol.* **2021**, *2353*, 259–280.
43. Liu, J.; Chakraborty, S.; Hosseinzadeh, P.; Yu, Y.; Tian, S.; Petrik, I.; Bhagi, A.; Lu, Y. Metalloproteins Containing Cytochrome, Iron-Sulfur, or Copper Redox Centers. *Chem. Rev.* **2014**, *114*, 4366–4469. [[CrossRef](#)] [[PubMed](#)]
44. Villalta, A.; Srour, B.; Lartigue, A.; Clémancey, M.; Byrne, D.; Chaspoul, F.; Loquet, A.; Guigliarelli, B.; Blondin, G.; Abergel, C.; et al. Evidence for [2Fe-2S]²⁺ and Linear [3Fe-4S]¹⁺ Clusters in a Unique Family of Glycine/Cysteine-Rich Fe-S Proteins from Megavirinae Giant Viruses. *J. Am. Chem. Soc.* **2023**, *145*, 2733–2738. [[CrossRef](#)] [[PubMed](#)]
45. Smith, A.T.; Linkous, R.O.; Max, N.J.; Sestok, A.E.; Szalai, V.A.; Chacón, K.N. The FeoC [4Fe-4S] cluster is redox-active and rapidly oxygen-sensitive. *Biochemistry* **2019**, *58*, 4935–4949. [[CrossRef](#)]
46. Lillig, C.H.; Berndt, C.; Vergnolle, O.; Lönn, M.E.; Hudemann, C.; Bill, E.; Holmgren, A. Characterization of human glutaredoxin 2 as iron-sulfur protein: A possible role as redox sensor. *Proc. Natl. Acad. Sci. USA* **2005**, *102*, 8168–8173. [[CrossRef](#)] [[PubMed](#)]
47. Brown, A.C.; Suess, D.L.M. An Open-Cuboidal [Fe₃S₄] Cluster Characterized in Both Biologically Relevant Redox States. *J. Am. Chem. Soc.* **2023**, *145*, 2075–2080. [[CrossRef](#)] [[PubMed](#)]
48. Elgrishi, N.; Rountree, K.J.; McCarthy, B.D.; Rountree, E.S.; Eisenhart, T.T.; Dempsey, J.L. A Practical Beginner's Guide to Cyclic Voltammetry. *J. Chem. Educ.* **2018**, *95*, 197–206. [[CrossRef](#)]
49. Bak, D.W.; Elliott, S.J. Alternative FeS cluster ligands: Tuning redox potentials and chemistry. *Curr. Opin. Chem. Biol.* **2014**, *19*, 50–58. [[CrossRef](#)]
50. Zanello, P. The competition between chemistry and biology in assembling iron-sulfur derivatives. Molecular structures and electrochemistry. Part II. {[Fe₂S₂](S^YCys)₄} proteins. *Coord. Chem. Rev.* **2014**, *280*, 54–83. [[CrossRef](#)]
51. Nano, A.; Furst, A.L.; Hill, M.G.; Barton, J.K. DNA electrochemistry: Charge-transport pathways through DNA films on gold. *J. Am. Chem. Soc.* **2021**, *143*, 11631–11640. [[CrossRef](#)]
52. Jones, J.E.; Le Sage, V.; Lakdawala, S.S. Viral and host heterogeneity and their effects on the viral life cycle. *Nat. Rev. Microbiol.* **2021**, *19*, 272–282. [[CrossRef](#)]
53. Dixit, H.; Kulharia, M.; Verma, S.K. Metalloproteome of human-infective RNA viruses: A study towards understanding the role of metal ions in virology. *Pathog. Dis.* **2023**, *81*, ftad020. [[CrossRef](#)]
54. Chen, A.Y.; Adamek, R.N.; Dick, B.L.; Credille, C.V.; Morrison, C.N.; Cohen, S.M. Targeting Metalloenzymes for Therapeutic Intervention. *Chem. Rev.* **2019**, *119*, 1323–1455. [[CrossRef](#)] [[PubMed](#)]
55. Zhu, H.; Cong, J.P.; Shenk, T. Use of differential display analysis to assess the effect of human cytomegalovirus infection on the accumulation of cellular RNAs: Induction of interferon-responsive RNAs. *Proc. Natl. Acad. Sci. USA* **1997**, *94*, 13985–13990. [[CrossRef](#)] [[PubMed](#)]
56. Gizzi, A.S.; Grove, T.L.; Arnold, J.J.; Jose, J.; Jangra, R.K.; Garforth, S.J.; Du, Q.; Cahill, S.M.; Dulyaninova, N.G.; Love, J.D.; et al. A naturally occurring antiviral ribonucleotide encoded by the human genome. *Nature* **2018**, *558*, 610–614. [[CrossRef](#)] [[PubMed](#)]
57. Shaveta, G.; Shi, J.; Chow, V.T.K.; Song, J. Structural characterization reveals that viperin is a radical S-adenosyl-l-methionine (SAM) enzyme. *J. Biochem. Biophys. Res. Commun.* **2010**, *391*, 1390–1395. [[CrossRef](#)] [[PubMed](#)]
58. Duschene, K.S.; Broderick, J.B. The antiviral protein viperin is a radical SAM enzyme. *FEBS Lett.* **2010**, *584*, 1263–1267. [[CrossRef](#)] [[PubMed](#)]
59. Hu, L.; Crawford, S.E.; Hyser, J.M.; Estes, M.K.; Prasad, B.V. Rotavirus non-structural proteins: Structure and function. *Curr. Opin. Virol.* **2012**, *2*, 380–388. [[CrossRef](#)]
60. Martin, D.; Charpillionne, A.; Parent, A.; Boussac, A.; D'Autreaux, B.; Poupon, J.; Poncet, D. The rotavirus nonstructural protein NSP5 coordinates a [2Fe-2S] iron-sulfur cluster that modulates interaction to RNA. *FASEB J.* **2013**, *27*, 1074–1083. [[CrossRef](#)]

61. Boothpur, R.; Brennan, D.C. Human polyoma viruses and disease with emphasis on clinical BK and JC. *J. Clin. Virol.* **2010**, *47*, 306–312. [[CrossRef](#)]
62. Tsang, S.H.; Wang, R.; Nakamaru-Ogiso, E.; Knight, S.A.; Buck, C.B.; You, J. The Oncogenic Small Tumor Antigen of Merkel Cell Polyomavirus Is an Iron-Sulfur Cluster Protein That Enhances Viral DNA Replication. *J. Virol.* **2015**, *90*, 1544–1556. [[CrossRef](#)]
63. Tan, M.; Bhadoria, A.S.; Cui, F.; Tan, A.; Van Holten, J.; Easterbrook, P.; Ford, N.; Han, Q.; Lu, Y.; Bulterys, M.; et al. Estimating the proportion of people with chronic hepatitis B virus infection eligible for hepatitis B antiviral treatment worldwide: A systematic review and meta-analysis. *Lancet Gastroenterol. Hepatol.* **2021**, *6*, 106–119. [[CrossRef](#)] [[PubMed](#)]
64. Jiang, T.; Liu, M.; Wu, J.; Shi, Y. Structural and biochemical analysis of Bcl-2 interaction with the hepatitis B virus protein HBx. *Proc. Natl. Acad. Sci. USA* **2016**, *113*, 2074–2079. [[CrossRef](#)]
65. Alvarez, S.W.; Sviderskiy, V.O.; Terzi, E.M.; Papagiannakopoulos, T.; Moreira, A.L.; Adams, S.; Sabatini, D.M.; Birsoy, K.; Possemato, R. NFS1 undergoes positive selection in lung tumours and protects cells from ferroptosis. *Nature* **2017**, *551*, 639–643. [[CrossRef](#)] [[PubMed](#)]
66. Petronek, M.S.; Spitz, D.R.; Allen, B.G. Iron-Sulfur Cluster Biogenesis as a Critical Target in Cancer. *Antioxidants* **2021**, *10*, 1458. [[CrossRef](#)] [[PubMed](#)]
67. La Scola, B.; Audic, S.; Robert, C.; Jungang, L.; de Lamballerie, X.; Drancourt, M.; Birtles, R.; Claverie, J.M.; Raoult, D. A giant virus in amoebae. *Science* **2003**, *299*, 2033. [[CrossRef](#)] [[PubMed](#)]
68. Peiris, J.S.; Lai, S.T.; Poon, L.L.; Guan, Y.; Yam, L.Y.; Lim, W.; Nicholls, J.; Yee, W.K.; Yan, W.W.; Cheung, M.T.; et al. SARS study group. Coronavirus as a possible cause of severe acute respiratory syndrome. *Lancet* **2003**, *361*, 1319–1325. [[CrossRef](#)] [[PubMed](#)]
69. Guan, Y.; Zheng, B.J.; He, Y.Q.; Liu, X.L.; Zhuang, Z.X.; Cheung, C.L.; Luo, S.W.; Li, P.H.; Zhang, L.J.; Guan, Y.J.; et al. Isolation and characterization of viruses related to the SARS coronavirus from animals in southern China. *Science* **2003**, *302*, 276–278. [[CrossRef](#)]
70. Assiri, A.; McGeer, A.; Perl, T.M.; Price, C.S.; Al Rabeeah, A.A.; Cummings, D.A.; Alabdullatif, Z.N.; Assad, M.; Almulhim, A.; Makhdoom, H.; et al. Hospital outbreak of Middle East respiratory syndrome coronavirus. *N. Engl. J. Med.* **2013**, *369*, 407–416. [[CrossRef](#)]
71. Gao, Y.; Yan, L.; Huang, Y.; Liu, F.; Zhao, Y.; Cao, L.; Wang, T.; Sun, Q.; Ming, Z.; Zhang, L.; et al. Structure of the RNA-dependent RNA polymerase from COVID-19 virus. *Science* **2020**, *368*, 779–782. [[CrossRef](#)]
72. Vernis, L.; El Banna, N.; Baille, D.; Hatem, E.; Heneman, A.; Huang, M.E. Fe-S Clusters Emerging as Targets of Therapeutic Drugs. *Oxid. Med. Cell. Longev.* **2017**, *2017*, 3647657. [[CrossRef](#)]
73. Davis, N.K.; Chater, K.F. The *Streptomyces coelicolor* whiB gene encodes a small transcription factor-like protein dispensable for growth but essential for sporulation. *Mol. Gen. Genet.* **1992**, *232*, 351–358. [[CrossRef](#)] [[PubMed](#)]
74. Morris, R.P.; Nguyen, L.; Gatfield, J.; Visconti, K.; Nguyen, K.; Schnappinger, D.; Ehrt, S.; Liu, Y.; Heifets, L.; Pieters, J.; et al. Ancestral antibiotic resistance in *Mycobacterium tuberculosis*. *Proc. Natl. Acad. Sci. USA* **2005**, *102*, 12200–12205. [[CrossRef](#)] [[PubMed](#)]
75. Wan, T.; Horová, M.; Khetrapal, V.; Li, S.; Jones, C.; Schacht, A.; Sun, X.; Zhang, L. Structural basis of DNA binding by the WhiB-like transcription factor WhiB3 in *Mycobacterium tuberculosis*. *J. Biol. Chem.* **2023**, *299*, 104777. [[CrossRef](#)] [[PubMed](#)]
76. Seo, S.; Kim, D.; Latif, H.; O'Brien, E.J.; Szubin, R.; Palsson, B.O. Deciphering Fur transcriptional regulatory network highlights its complex role beyond iron metabolism in *Escherichia coli*. *Nat. Commun.* **2014**, *5*, 4910. [[CrossRef](#)] [[PubMed](#)]
77. Fillat, M.F. The FUR (ferric uptake regulator) superfamily: Diversity and versatility of key transcriptional regulators. *Arch. Biochem. Biophys.* **2014**, *546*, 41–52. [[CrossRef](#)] [[PubMed](#)]
78. Fontenot, C.R.; Tasnim, H.; Valdes, K.A.; Popescu, C.V.; Ding, H. Ferric uptake regulator (Fur) reversibly binds a [2Fe-2S] cluster to sense intracellular iron homeostasis in *Escherichia coli*. *J. Biol. Chem.* **2020**, *295*, 15454–15463. [[CrossRef](#)] [[PubMed](#)]
79. Cartron, M.L.; Maddocks, S.; Gillingham, P.; Craven, C.J.; Andrews, S.C. Feo—Transport of ferrous iron into bacteria. *Biomaterials* **2006**, *19*, 143–157. [[CrossRef](#)]
80. Andrews, S.C.; Robinson, A.K.; Rodríguez-Quiñones, F. Bacterial iron homeostasis. *FEMS Microbiol. Rev.* **2003**, *27*, 215–337. [[CrossRef](#)]
81. Cornelis, P.; Dingemans, J. *Pseudomonas aeruginosa* adapts its iron uptake strategies in function of the type of infections. *Front. Cell. Infect. Microbiol.* **2013**, *3*, 75. [[CrossRef](#)]
82. Hsueh, K.L.; Yu, L.K.; Chen, Y.H.; Cheng, Y.H.; Hsieh, Y.C.; Ke, S.C.; Hung, K.W.; Chen, C.J.; Huang, T.H. FeoC from *Klebsiella pneumoniae* contains a [4Fe-4S] cluster. *J. Bacteriol.* **2013**, *195*, 4726–4734. [[CrossRef](#)]
83. Hsueh, K.L.; Yu, L.K.; Hsieh, Y.C.; Hsiao, Y.Y.; Chen, C.J. FeoC from *Klebsiella pneumoniae* uses its iron sulfur cluster to regulate the GTPase activity of the ferrous iron channel. *Biochim. Biophys. Acta Proteins Proteom.* **2023**, *1871*, 140855. [[CrossRef](#)] [[PubMed](#)]

Disclaimer/Publisher's Note: The statements, opinions and data contained in all publications are solely those of the individual author(s) and contributor(s) and not of MDPI and/or the editor(s). MDPI and/or the editor(s) disclaim responsibility for any injury to people or property resulting from any ideas, methods, instructions or products referred to in the content.